



1 An Evaluation of the Performance of Sea-Bird Scientific's Autonomous SeaFET™:  
2 Considerations for the Broader Oceanographic Community

3

4 Cale A. Miller<sup>1,3</sup>, Katie Pocock<sup>2</sup>, Wiley Evans<sup>2</sup>, and Amanda L. Kelley<sup>1\*</sup>

5

6 1. College of Fisheries and Ocean Sciences, University of Alaska Fairbanks, Fairbanks, AK,  
7 USA

8

9 2. Hakai Institute, Heriot Bay, BC, Canada

10

11 3. **Present address:** Department of Evolution and Ecology, College of Biological Sciences,  
12 University of California Davis, CA, USA

13

14 \*Correspondence to: Amanda L. Kelley ([alkelley@alaska.edu](mailto:alkelley@alaska.edu))

15

16

## 17 Abstract

18

19 The commercially available Sea-Bird SeaFET™ provides an accessible way for a broad  
20 community of researchers to study ocean acidification and obtain robust measurements of  
21 seawater pH via the use of an *in situ* autonomous sensor. There are pitfalls, however, that have  
22 been detailed in previous best practices for sensor care, deployment, and data handling. Here, we  
23 took advantage of two distinctly different coastal settings to evaluate the Sea-Bird SeaFET™ and  
24 examine the multitude of scenarios in which problems may arise confounding the accuracy of  
25 measured pH. High-resolution temporal measurements of pH were obtained during 3- to 5-month  
26 field deployments in three separate locations (two in south-central, Alaska, USA, and one British  
27 Columbia, Canada) spanning a broad range of nearshore temperature and salinity conditions.  
28 Both the internal and external electrodes onboard the SeaFET™ were evaluated against robust  
29 benchtop measurements for accuracy utilizing either the factory calibration, an *in situ* single-  
30 point calibration, or *in situ* multi-point calibration. In addition, two sensors deployed in parallel  
31 in Kasitsna Bay, AK, USA, were compared for inter-sensor variability in order to quantify other  
32 factors contributing to SeaFET™ intrinsic inaccuracies. Based on our results, the multi-point  
33 calibration method provided the highest accuracy (< 0.025 difference in pH) of pH when  
34 compared against benchtop measurements. Spectral analysis of time series data showed that  
35 during spring in Alaskan waters, a range of tidal frequencies dominated pH variability, while  
36 seasonal oceanographic conditions were the dominant driver in Canadian waters. Further, it is  
37 suggested that spectral analysis performed on initial deployments may be able to act as an *a*  
38 *posteriori* method to better identify appropriate calibration regimes. Based on this evaluation, we  
39 provide a comprehensive assessment of the potential sources of uncertainty associated with  
40 accuracy and precision of the SeaFETs™ electrodes.

41

## 42 1 Introduction

43

44 The intrusion of excess anthropogenic CO<sub>2</sub> into the global oceans—referred to as ocean  
45 acidification (OA)—induces a series of geochemical reactions that increases seawater [H<sup>+</sup>]  
46 (lowering pH) while concomitantly reducing the ocean's overall buffering capacity by reducing



47 the  $[\text{CO}_3^{2-}]$  (Caldeira and Wickett, 2003; Orr et al., 2005). Due to more dynamic natural physical  
48 and chemical processes in the coastal ocean, a differentiation exists between open-ocean  
49 acidification and nearshore coastal acidification. Open-ocean acidification of surface waters is  
50 predominately a function of equilibration with atmospheric  $p\text{CO}_2$ , thus increasing on yearly and  
51 decadal timescales as continued burning of fossil fuels ensues (Hofmann et al., 2011; Orr et al.,  
52 2005). Coastal acidification, however, can manifest on short time and space scales driven by  
53 riverine input and its chemical constituents (e.g., organic carbon, nutrients, and organic  
54 alkalinity), community metabolism and organization, tidal cycles, upwelling, and groundwater  
55 input (Duarte et al., 2013; Sunda and Cai, 2012; Waldbusser and Salisbury, 2014), all of which  
56 can act in conjunction with increasing atmospheric  $\text{CO}_2$ , leading to more frequent, intense, and  
57 longer-lasting acidification events (Hales et al., 2016; Harris et al., 2013). In the face of rapidly  
58 changing coastal conditions, tracking and quantifying the progression of OA requires precise and  
59 accurate measurements of carbonate chemistry over long periods of time; these can be achieved  
60 by appropriately constraining the carbonate system by measuring at least two of the system's  
61 parameters: total dissolved inorganic carbon ( $\text{TCO}_2$ ), total alkalinity (TA), pH, and the partial  
62 pressure of  $\text{CO}_2$  ( $p\text{CO}_2$ ). Despite the marked increase in OA research over the past decade  
63 (Riebesell and Gattuso, 2015; Rudd, 2017), nearshore monitoring efforts—particularly in  
64 estuarine waters—have been slow to ramp up, however, efforts are beginning to intensify as  
65 technological advancements are made (Feely et al., 2010, 2016; Hales et al., 2016; Harris et al.,  
66 2013; Newton et al., 2012; Waldbusser and Salisbury, 2014; Chan et al., 2017).

67  
68 Acidification of Alaskan coastal waters is predicted to progress rapidly relative to other  
69 regions within the next 50 years, and negatively impact the social-ecological structure of Alaskan  
70 marine resources by disrupting the Alaska Native subsistence and commercial fisheries (Ekstrom  
71 et al., 2015; Mathis et al., 2015b). The ocean waters present along the Alaskan coastline  
72 experience chemical and physical drivers of seawater chemistry that are unique to this region.  
73 The low seawater temperatures inherently have higher concentrations of dissolved  $\text{CO}_2$ , and  
74 chemical and physical oceanic processes unique to Alaskan waters such as sea ice melt, glacial  
75 discharge, and benthic pelagic coupling across shallow shelves are likely to exacerbate  
76 acidification in this region (Evans et al., 2014; Mathis et al., 2011a, 2011b, 2012). Recently, an  
77 OA monitoring initiative has been setup by the Alaska Ocean Observing Network (AOOS) to  
78 track and provide accessible material dedicated to acidification research in Alaskan waters  
79 (<http://www.aos.org/alaska-ocean-acidification-network>). Along the Pacific coast of Alaska, a  
80 robust benchtop system known as a Burke-o-Lator (BoL), which measures  $\text{TCO}_2$  and  $p\text{CO}_2$   
81 either continuously in a flow-through environment or from discrete seawater samples (Bandstra  
82 et al., 2006; Barton et al., 2012; Hales et al., 2016) has been installed in several locations,  
83 including the OceansAlaska Shellfish Hatchery in Ketchikan, the Alutiiq Pride Shellfish  
84 Hatchery in Seward (Evans et al., 2015), and at the Sitka Tribe of Alaska Environmental  
85 Research Center (real-time data from Alaskan and other BoLs:  
86 [http://www.ipacoa.org/Explorer?action=oiw:fixed\\_platform](http://www.ipacoa.org/Explorer?action=oiw:fixed_platform)). Nominal analytical uncertainty for  
87  $\text{TCO}_2$  determinations from this system is 0.2% based on the reproducibility of sample and  
88 certified reference material (CRM; provided by A. Dickson analyses). For  $p\text{CO}_2$  determinations,  
89 analytical uncertainty is 1.5% based on the inaccuracy of calculated CRM alkalinity relative to  
90 the certified value. While the BoL has significant advantages for achieving robust OA  
91 measurements in nearshore waters, the physical constraints of a benchtop system limit the spatial  
92 dimension of which carbonate chemistry parameters can be measured. One potential resolution



93 to diminish the gap in coverage of OA monitoring is to utilize autonomous pH sensors, which are  
94 far more versatile in their ability to monitor hard-to-reach areas.

95  
96 Recent assessments regarding OA monitoring efforts have specifically highlighted the  
97 benefits of accessibility by the commercially produced SeaFET<sup>TM</sup> pH sensor utilizing Honeywell  
98 Durafet technology (Martz et al., 2015). The SeaFET<sup>TM</sup> was originally developed at the  
99 Monterey Bay Aquarium Research Institute (Martz et al., 2010), but since has been  
100 manufactured and distributed by Satlantic (<http://www.satlantic.com>), which is now incorporated  
101 into Sea-Bird Scientific (<http://www.seabird.com>). The partnership between MBARI, Scripps  
102 Institute of Oceanography, and Satlantic led the way for commercial availability of the  
103 SeaFET<sup>TM</sup>, providing a ready-to-deploy-factory calibration, quick start manual, and user-friendly  
104 interface. The first generation of SeaFETs<sup>TM</sup> (not distributed by Sea-Bird, but by Dr. Todd Martz  
105 at Scripps Institute of Oceanography) have been deployed in numerous field studies and were  
106 heavily scrutinized in order to provide robust best practices for appropriate calibration and  
107 deployment procedures (Bresnahan et al., 2014; Hofmann et al., 2011; Kapsenberg and  
108 Hofmann, 2016; Martz et al., 2010; Matson et al., 2011; Yu et al., 2011). More recent studies  
109 have expanded the scope of SeaFET<sup>TM</sup> accuracy, inter-sensor variability, operator experience,  
110 and multi-point calibration techniques (Gonski et al., 2018; Johnson et al., 2017; Kapsenberg et  
111 al., 2017; McLaughlin et al., 2017). Given the multitude of information regarding SeaFET<sup>TM</sup>  
112 performance, coalescing all the potential sources of uncertainty in measurements (e.g., inter-  
113 sensor variability and calibration method) can be logistically challenging for non-experienced  
114 oceanographers who now have access to the commercially available SeaFETs<sup>TM</sup> distributed by  
115 Sea-Bird.

116  
117 In this study, we aimed to take advantage of two distinct coastal settings in order to  
118 deploy and evaluate the commercially available Sea-Bird SeaFET<sup>TM</sup>, and the potential  
119 uncertainties that can arise with time series pH<sub>t</sub> (total scale) measurements. For this evaluation,  
120 SeaFETs<sup>TM</sup> were co-deployed side-by-side to quantify inter-sensor variability, discrepancies  
121 were examined between factory calibration, *in situ* single-point calibration, and *in situ* multi-  
122 point calibration pH<sub>t</sub> values, and anomalous data associated with SeaFET<sup>TM</sup> conditioning times  
123 were detailed and considered as potential sources of measurement inaccuracies. All evaluations  
124 of SeaFET<sup>TM</sup> performance were under non-controlled source water conditions or by *in situ*  
125 deployments. Three SeaFETs<sup>TM</sup> were deployed in coastal waters and were subjected to tidal  
126 influences and freshwater input, while a fourth was compared to pH<sub>t</sub> values derived from  
127 measurements obtained by a BoL. Finally, a spectral analysis of the quality-controlled data was  
128 performed in order to identify the driving mechanism of pH<sub>t</sub> variability between these divergent  
129 sites and consider possible un-accounted for calibration errors that could occur in dynamic  
130 settings that might not be resolved using a specific calibration method.

## 131 132 **2 Methods**

### 133 134 **2.1 Apparatus: SeaFET<sup>TM</sup>**

135  
136 The commercially available Sea-Bird SeaFET<sup>TM</sup> has retained the basic design of the original  
137 SeaFET<sup>TM</sup> developed at MBARI (Martz et al., 2010). The SeaFET<sup>TM</sup> utilizes the ion sensitive  
138 field effect transistor (ISFET) technology, and is outfitted with an internal Honeywell Durafet



139 and an external solid-state chloride selective electrode (Cl-ISE) along with an internal thermistor,  
 140 which derives temperature using the (Steinhart and Hart, 1968) equation. The internal reference  
 141 electrode is intrinsically insensitive to salinity over a tested range from 30 – 36 (Bresnahan et al.,  
 142 2014), with recent work even suggesting near-ideal Nernstian response to salinity as low as ~9.0  
 143 (Gonski et al., 2018). This is in converse to the chloride sensitive external electrode, which is  
 144 salinity dependent. Both electrodes demonstrate exceptional stability over a range of moderate  
 145 salinity (30 – 36) and broad temperature (-1 to 35 °C) (Bresnahan et al., 2014; Kapsenberg et al.,  
 146 2015; Martz et al., 2014, 2010). The range of salinity sensitivity for the external electrode has  
 147 even been extended down to 20, where it displays a near-ideal Nernst slope (Takeshita et al.,  
 148 2014). Sea-Bird suggests that the external reference electrode provides the more accurate and  
 149 stable  $pH_t$  measurement given that chloride concentration can be precisely determined from  
 150 accurate salinity measurements. This is in agreement with previous research demonstrating that  
 151 the external electrode has a more robust stability (Martz et al., 2010). In dynamic nearshore  
 152 environments (e.g., estuaries with strong tidal and riverine fluxes), however, the  $pH_t$  derived  
 153 from the internal electrode is recommended (Sea-Bird Scientific's Branham, C., pers. comm.)  
 154 despite the potential of thermodynamic hysteresis (Martz et al., 2010). Bresnahan et al. (2014)  
 155 demonstrated that the internal electrode is of the highest quality and under most scenarios  
 156 remains nearly as stable as the external electrode—this was further corroborated by Gonski et al.  
 157 (2018) with SeapHOx deployments in the Murderkill estuary, Delaware.

## 158 2.2 Calibration

159 Currently, three different calibration methods are present for the SeaFET<sup>TM</sup>: a factory pre-  
 160 deployment single-point calibration, *in situ* single-point calibration, and an *in situ* multi-point  
 161 calibration (Bresnahan et al., 2014; Gonski et al., 2018). To properly calculate  $pH_t$  from  
 162 SeaFET<sup>TM</sup> voltage readings, an appropriate calibration coefficient is required. The applied  
 163 calibration coefficients from the factory are a single-point, pre-deployment calibration. Given  
 164 that a conditioning period is required for the SeaFET<sup>TM</sup> (Bresnahan et al., 2014), these  
 165 coefficients are likely not adequate once the sensor becomes conditioned to the environment to  
 166 which it is deployed. For the internal electrode, the new calibration coefficient  $k_{0i}$  can be  
 167 determined as

$$171 \quad k_{0i} = -S_{Nernst} * pH_t + V_{int} - k_{2i} * T, \quad (1)$$

172 and  $k_{0e}$  for the external electrode

$$173 \quad k_{0e} = V_{ext} - pH_t + \log\left(1 + \frac{S_t}{K_s}\right) - 2 * \log(\gamma_{HCl}) - \log(Cl_T) * S_{nernst} + k_{2e} * T \quad (2)$$

174 where  $V_{FET}$  is the voltage from the electrode and  $k_2$  is the temperature coefficient ( $dE^*/dT$ )  
 175 applied to all SeaFETs<sup>TM</sup> (Martz et al., 2010). For detailed definitions of  $S_{nernst}$  and the salinity  
 176 dependent constants  $\gamma_{HCl}$  (HCl activity coefficient),  $Cl_T$  (total chloride),  $S_T$  (total sulfate), and the  
 177  $HSO_4^-$  dissociation constant  $K_s$  (Dickson et al., 2007; Khoo et al., 1977) in equations 1 and 2, we  
 178 refer readers to Martz et al. (2010), Bresnahan et al. (2014), and Sea-Bird Scientific SeaFET<sup>TM</sup>  
 179 Product Manual 2.0.0. In the literature, SeaFET<sup>TM</sup> calibration coefficients have been denoted as  
 180  $E_{int}^*$  and  $E_{ext}^*$  (Martz et al. 2010, Bresnahan et al. 2014), however, for the purpose of this



184 evaluation—which specifically examines commercially available Sea-Bird SeaFETs™—the  
185 adoption of  $k_0$  and  $k_2$  is in accordance with the preferred nomenclature from the manufacturer.

186

187

188 Unlike the factory pre-deployment single-point calibration, the *in situ* single-point  
189 calibration occurs after the sensor has been deployed in the field. At the operator’s discretion, a  
190 discrete sample will be collected in direct proximity to the deployed SeaFET™ at the same time  
191 that the sensor is actively making a measurement, and then measured for  $\text{pH}_t$  at *in situ*  
192 temperature and salinity. The known  $\text{pH}_t$  would then be used in the above equations as the “ $\text{pH}_t$ ”  
193 variable. Similar to the single-point *in situ* calibration, the multi-point calibration derives a series  
194 of calibration coefficients over a short period of time that is long enough to capture environment  
195 variability such as tidal fluxes, and then a single calibration coefficient is averaged. Both single-  
196 point calibration methods—pre-deployment and *in situ*—appear to be suitable for fairly static  
197 environmental conditions, whereas the multi-point *in situ* calibration is best suited for dynamic  
198 nearshore environments (Bresnahan et al., 2014; Gonski et al., 2018).

198

### 199 **2.3 SeaFET™ conditioning: test tank deployments**

200

201 A series of three separate test tank deployments for three SeaFETs™<sub>395, 396, 397</sub> were conducted in  
202 order to determine the conditioning period for each sensor. Initial sensor deployments took place  
203 in October 2016 at the Alutiiq Pride Shellfish Hatchery (APSH) in Seward, Alaska. Sensors were  
204 deployed for a duration of 72 hours in a flow-through 60 L tank where seawater taken from a  
205 depth of ~75 m in Resurrection Bay was sand-filtered, UV treated, and finally run through a 5  
206  $\mu\text{m}$  mesh. All three sensors were programmed with identical sampling settings (Table 1). The  
207 onboard internal thermistor was used to calculate temperature, and measurements of seawater  
208 salinity incoming to the hatchery were collected by a Sea-Bird Scientific SBE 45 MicroTSG  
209 Thermosalinograph that is paired with the BoL and are available on the Alaska Ocean Observing  
210 System (<http://portal.aos.org/real-time-sensors.php#map>). Factory calibration coefficients for  
211 the internal ( $k_{0i}$ ,  $k_{2i}$ ) and external ( $k_{0e}$ ,  $k_{2e}$ ) electrodes were retained when processing raw voltage  
212 data.

213

214 A second tank deployment for the same three SeaFETs™<sub>395, 396, 397</sub> were deployed at the  
215 University of Alaska, Fairbanks, in the Ocean Acidification Research Center (OARC). Seawater  
216 collected from the APSH was delivered to the OARC test tank, ~370 L in a half-filled tank.  
217 Seawater in the tank was circulated continuously and covered to aid in the prevention of  
218 evaporation and photosynthesis. A co-deployed Sea-Bird SBE 16plusV2 SeaCAT (recently  
219 serviced by Sea-Bird) collected temperature and salinity readings every 5 minutes.  
220 SeaFETs™<sub>395, 396, 397</sub> were deployed for a duration of nine days in continuous operation mode  
221 which forgoes the ability to set frames per burst; average number of reads was identical between  
222 all sensors (Table 1). From 1 – 4 November 2016, duplicate discrete bottle samples were  
223 collected in 250 ml glass bottles with screw caps at ~00:00 and 17:00 UTC per day. Bottle  
224 samples were preserved with 20  $\mu\text{l}$  of saturated  $\text{HgCl}_2$  and processed at a later date for  $\text{TCO}_2$  and  
225 TA with a VINDTA 3C (Versatile Instrument for the Determination of total inorganic carbon  
226 and titration alkalinity). The VINDTA 3C has an uncertainty typically near 0.05% (Mathis et al.,  
227 2014, 2015a). Bottle sample  $\text{pH}_t$  was calculated using CO2SYS with known  $\text{TCO}_2$  and TA using  
228 the constants provided by (Uppström, 1974) and (Lueker et al., 2000); derived  $\text{pH}_t$  was then  
229 compared against SeaFET™ sensor  $\text{pH}_t$  to test the accuracy of both internal and external



230 electrodes, assuming the discrete bottle samples were the “true pH” of the seawater. Upon  
231 recovery, all SeaFETs<sup>TM</sup><sub>395, 396, 397</sub> were placed into polled mode and stored with wet caps filled  
232 with tris buffer (salinity 34, pH 8.09 at room temperature, 25 °C). Again, the factory calibration  
233 coefficients for the internal and external electrodes were retained when raw voltage was  
234 processed. Since the SBE 16plusV2 sampled every 5 min, salinity and temperature measured by  
235 the SBE at each 5-minute point was repeated for the following 4 minutes in order to calculate  
236 continuous minute readings by SeaFETs<sup>TM</sup><sub>395, 396, 397</sub>.

237

238 A final test tank deployment of the SeaFETs<sup>TM</sup><sub>395, 396, 397</sub> at OARC was conducted after an  
239 assumed adequate conditioning period of nine days (first OARC deployment). All three  
240 SeaFETs<sup>TM</sup><sub>395, 396, 397</sub> had been set to polled mode after the end of the previous deployment and,  
241 therefore, were sleeping for 83 days until this final seven day deployment. The sampling settings  
242 were identical to the first OARC deployment for all three SeaFETs<sup>TM</sup><sub>395, 396, 397</sub> (Table 1). Similar  
243 to the previous OARC tank deployment, a co-deployed Sea-Bird SBE 16plusV2 SeaCAT  
244 collected temperature and salinity mirroring the SeaFET sampling interval of 3 hrs.

245

246 The internal thermistor of each SeaFET<sup>TM</sup><sub>395, 396, 397</sub> was tested for accuracy by comparing  
247 its derived *in situ* temperature to that collected by the Sea-Bird SBE 16plusV2 during the test  
248 tank deployments. The temperature difference between the internal thermistor and the SBE  
249 16plusV2 was used to calculate the average and maximum discrepancy between the two  
250 temperature readings. The temperature discrepancy was then applied to a combination of TA:  
251 TCO<sub>2</sub> ratios over a range of salinity (20 – 35) in CO2SYS (constants: Uppström, 1974; Lueker et  
252 al., 2000), which produced two different pH<sub>t</sub> values. The difference between these two pH<sub>t</sub>  
253 values were, therefore, concluded to be a result of the temperature discrepancy.

254

## 255 2.4 SeaFET<sup>TM</sup> performance: field deployments

256

257 In late winter 2017—32 days post final tank deployment—SeaFET<sup>TM</sup><sub>397</sub> was deployed at the  
258 APSH and the two remaining sensors (SeaFET<sup>TM</sup><sub>395, 396</sub>) in Kasitsna Bay within greater  
259 Kachemak Bay, Alaska (Fig. 1). At the APSH (60° 5' 55.59"N, 149° 26' 39.80"W), incoming  
260 seawater from Resurrection Bay at a depth of 75 m is split before running through a series of  
261 hatchery water filters so that an unfiltered line is run directly to the BoL. The incoming line to  
262 the BoL was then split to feed an ~11.5 L conical tank housing the SeaFET<sup>TM</sup><sub>397</sub> fit with the  
263 copper bio-fouling guard; tank residence time was ~7.5 min. The SeaFET<sup>TM</sup><sub>397</sub> at this location  
264 was deployed on 6 March 2017 with a robust sampling setting (Table 1). Two calibration  
265 methods were applied for this SeaFET<sup>TM</sup><sub>397</sub>, an *in situ* single-point calibration and an *in situ*  
266 multi-point calibration. Both calibrations were performed 50 days after deployment on 25 April  
267 2017 once the BoL had completed service maintenance. The single-point *in situ* calibration was  
268 taken during midday tide transition in Resurrection Bay, while the multi-point *in situ* approach  
269 used five (sensor sampling 3 h intervals) time points spanning an entire tidal cycle. The single-  
270 point *in situ* calibration was used to derive  $k_{0i}$  for the internal electrode (eq. 1) and  $k_{0e}$  for the  
271 external electrode (eq. 2). The multi-point *in situ* calibration followed the same formulations  
272 with the difference being the final calibration coefficient calculated was the average of the five  
273 independently calculated calibration coefficients. Three final pH<sub>t</sub> values for the SeaFET<sup>TM</sup><sub>397</sub>  
274 were, therefore, calculated based upon the different calibration coefficients (factory, single-point  
275 and multi-point *in situ* calibration) and compared against the pH<sub>t</sub> determined from continuous



276  $p\text{CO}_2$  measurements by the BoL and derived TA (TA-S equation, Evans et al. 2015) using  
277 CO2SYS with constants provided by Uppström (1974) and Lueker et al. (2000).  $\text{pH}_t$  uncertainty  
278 from the BoL using this combination of measured and derived parameters is 0.007 units based on  
279 propagating the error of the BoL  $p\text{CO}_2$  uncertainty reported above with the RMSE ( $17 \mu\text{mol kg}^{-1}$ )  
280 of the regional TA-S relationship (Orr, et al., *in prep*).  
281

282 Inter-sensor variability was examined between two SeaFETs<sup>TM</sup><sub>395, 396</sub> deployed off the  
283 pier at the Kasitsna Bay laboratory in Kachemak Bay ( $59^\circ 28' 6.71''\text{N}$ ,  $151^\circ 33' 11.12''\text{W}$ )  $\sim 1.5$  m  
284 from the bottom: depth at this location fluctuates between  $\sim 7.5 - 16.8$  m (Fig. 1). On 18 March  
285 2017—44 days post final tank deployment—SeaFETs<sup>TM</sup><sub>395, 396</sub> were attached to the pier piling  
286 directly beside one another on a single mooring frame. Both SeaFETs<sup>TM</sup> were wrapped with pipe  
287 tape to minimize biofouling and fit with their respective copper biofouling guards which had a  
288 tributyltin plug attached to the inside of the guard. The sampling settings for both SeaFETs<sup>TM</sup><sub>395,</sub>  
289 <sub>396</sub> were identical to the one at the APSH (Table 1). Five discrete reference samples were taken in  
290 duplicate: one sample on day of deployment (UTC: 3-18-17, 18:00), two samples 1-day post-  
291 deployment (UTC: 19 March 2017, 03:00 and 15:00), and two samples 2- and 1-day pre-  
292 recovery of the SeaFETs<sup>TM</sup><sub>395, 396</sub> (UTC 3 June 2017, 03:00; 6 June 2017, 03:00). Reference  
293 samples were collected within 30 s of the instrument sampling time period via a diver's hand  
294 Niskin, measured for temperature and salinity with a YSI 3100 conductivity instrument, stored in  
295 250 ml glass bottles with screw caps, poisoned with 100  $\mu\text{l}$  of saturated  $\text{HgCl}_2$ , and secured with  
296 teflon tape around the bottleneck threading and Parafilm wrapped on the outside of the cap.  
297 Calibration samples were processed for  $\text{TCO}_2$  and TA with a VINDTA 3C and  $\text{pH}_t$  calculated  
298 using CO2SYS with the constants provided by Uppström (1974) and Lueker et al. (2000).  
299 Salinity measurements collected by the Kachemak Bay National Estuarine Research Reserve  
300 data sonde, 10 km SE of the deployed sensors ( $59^\circ 26' 26.87''\text{N}$ ,  $151^\circ 43' 15.21''\text{W}$ ), were used  
301 along with the SeaFET's<sup>TM</sup> internal thermistor readings to calculate  $\text{pH}_t$  from the raw voltage  
302 data in order to capture representative environmental conditions providing relevance for the  $\text{pH}_t$   
303 time series in this location. A static salinity of 32 was also used for all calculations of  $\text{pH}_t$  as an  
304 assessment of variability due to salinity measured from a data sonde 10 km away. A total of four  
305 different  $\text{pH}_t$  values for both SeaFETs<sup>TM</sup><sub>395, 396</sub> were calculated based on calibration method  
306 (factory pre-deployment single-point calibration and the *in situ* single-point) and conditioning:  
307 either conditioned or non-conditioned to the environment. All calculated  $\text{pH}_t$  values from the  
308 SeaFETs<sup>TM</sup><sub>395, 396</sub> were then compared against the remaining discrete reference bottle samples  
309 not used for calibration. This was done in order to examine the accuracy and inter-sensor  
310 variability difference between conditioned and non-conditioned to the environment electrodes.  
311 Because the Kachemak Bay data sonde was located 10 km from the deployed SeaFETs<sup>TM</sup><sub>395, 396</sub>,  
312 the measured temperature and salinity from the discrete reference samples were used to  
313 determine  $\text{pH}_t$  for the internal and external electrodes at those specific time points. That is,  
314 sensor accuracy for these two SeaFETs<sup>TM</sup><sub>395, 396</sub> was only assessed with accurate temperature and  
315 salinity values determined from the discrete bottle samples.  
316

317 A fourth SeaFET<sup>TM</sup><sub>268</sub> operated by the Hakai Institute was deployed on Environment  
318 Canada's Sentry Shoal weather buoy in the Northern Strait of Georgia, BC, Canada:  $49^\circ 54'$   
319  $24.00''\text{N}$ ,  $124^\circ 59' 5.99''\text{W}$  (Fig. 1). The Sentry Shoal mooring site is in a water depth of 15 m and  
320 the SeaFET<sup>TM</sup><sub>268</sub> was affixed at a depth of 1 m. A pre-deployment bucket test was conducted for  
321 24 h at a sampling interval of 30 min with an average of 10 samples per frame and 30 frames per



322 burst from 28 – 29 June 2016. SeaFET<sup>TM</sup><sub>268</sub> was outfitted with a copper housing guard and  
 323 wrapped with copper tape. Sensor underwent two separate deployments, an initial deployment,  
 324 and a redeployment (6 July and 27 August 2016) that occurred after the sensor was retrieved for  
 325 cleaning and maintenance. Two separate calibration samples (taken in triplicate) were taken in  
 326 accordance with each deployment, and occurred 13 and 7 days after each deployment (19 July  
 327 and 2 September 2016). For each deployment, SeaFET<sup>TM</sup><sub>268</sub> settings were similar to the others at  
 328 the APSH and in Kasitsna Bay (Table 1). All calibration samples were taken in triplicate at a  
 329 depth of 1 m via CTD and Niskin bottle castings and collected in 350 ml amber glass bottles with  
 330 polyurethane-lined crimp-sealed metal caps and poisoned with 200 µl of saturated HgCl<sub>2</sub>, and  
 331 then processed for TCO<sub>2</sub> and pCO<sub>2</sub> with a BoL at the Hakai Institute's Quadra Island Field  
 332 Station. The measured values were used to derive pH<sub>t</sub> using CO2SYS with the constants  
 333 provided by (Uppström, 1974) and (Lueker et al., 2000) in order to perform a single-point *in situ*  
 334 calibration. Uncertainty in pH determinations from BoL pCO<sub>2</sub> and TCO<sub>2</sub> measurements was  
 335 0.006 units. After SeaFET<sup>TM</sup><sub>268</sub> deployment and calibration, a total of three, triplicate, reference  
 336 sample sets were taken and processed for pH<sub>t</sub> following the procedure used for calibration  
 337 samples, then compared against SeaFET pH<sub>t</sub>.

## 338 2.5 Quantifying pH<sub>t</sub> and intrinsic sensor uncertainties

339

340 Calculating pH<sub>t</sub> from the SeaFET's<sup>TM</sup> raw voltage reading is dependent on temperature, salinity  
 341 and an ideal 100% Nernstian response. The software application SeaFETcom permits the  
 342 operator to automatically calculate pH<sub>t</sub> by assigning the calibration coefficient either written to  
 343 the sensor's header file or the one provided on the CD-ROM (these should be identical).  
 344 Determination of final pH<sub>t</sub> values from the first test tank deployment at the APSH were  
 345 calculated by two different operators and two sources for the factory pre-deployment single-point  
 346 calibration coefficients: header file and CD-ROM disc file. Aside from that exception, all other  
 347 final pH<sub>t</sub> values for the internal and external electrodes were calculated with the Mathworks  
 348 software MATLAB (V. 2016a) and Microsoft excel (v. 2016) using the following equations for  
 349 the internal electrode

350

$$351 \quad pH_{int} = \frac{V_{FET|INT} - k_{0i} - k_{2i} * T}{S_{nernst}}, \quad (3)$$

352 and the external electrode

$$353 \quad pH_{ext} = \frac{V_{FET|EXT} - k_{0e} - k_{2e} * T}{S_{nernst}} + \log(Cl_T) + 2 * \log(\gamma_{HCl}) - \log\left(1 + \frac{S_t}{K_s}\right) \quad (4)$$

354 where V<sub>FET</sub> is the voltage from the electrode and k<sub>2</sub> is the temperature coefficient (dE\*/dT)  
 355 applied to all SeaFETs<sup>TM</sup> (Martz et al. 2010). Again, for detailed definitions of S<sub>nernst</sub> and the  
 356 salinity dependent constants γ<sub>HCl</sub> (HCl activity coefficient), Cl<sub>T</sub> (total chloride), S<sub>t</sub> (total sulfate),  
 357 and the HSO<sub>4</sub><sup>-</sup> dissociation constant K<sub>s</sub> (Khoo et al. 1977, Dickson et al. 2007) in equations 3 and  
 358 4, we refer readers to Martz et al. (2010), Bresnahan et al. (2014), and Sea-Bird Scientific  
 359 SeaFET<sup>TM</sup> Product Manual 2.0.0.

### 360 2.5.1 Sensor uncertainty

361 The overall accuracy (i.e., integrated uncertainties) of every SeaFET<sup>TM</sup> sensor was evaluated by





362 quantifying all sources of potential uncertainty when calculating a final  $\text{pH}_t$  from the SeaFET<sup>TM</sup>.  
363 The  $\text{pH}_t$  uncertainty introduced by calibration method was calculated as the absolute difference  
364 between the “true  $\text{pH}_t$ ” and the final sensor  $\text{pH}_t$  derived from either factory calibration, the  
365 single-point *in situ* calibration, or multi-point *in situ* calibration. The “true  $\text{pH}_t$ ” was calculated  
366 using CO2SYS dissociation constants by Lueker et al., (2000) and Uppström, (1974) with  
367 measured  $\text{TCO}_2$  and TA via the VINDTA 3C,  $\text{TCO}_2$  and  $p\text{CO}_2$  measured by the BoL for discrete  
368 samples (e.g., SeaFET<sup>TM</sup><sub>268</sub>), and  $p\text{CO}_2$  and TA (TA-S equation, Evans et al. 2015) for  
369 continuous samples (SeaFET<sup>TM</sup><sub>397</sub>). A one-way analysis of variance (ANOVA) and the root  
370 mean square error (RMSE) were run and calculated in order to compare the  $\text{pH}_t$  values from both  
371 electrodes on SeaFET<sup>TM</sup><sub>397</sub> across calibration methods against the  $\text{pH}_t$  values from the BoL. The  
372 BoL at the APSH sampled every 5 min which produced 256 comparable sample points with a  
373 time alignment disparity that ranged from 0 – 120 s against SeaFET<sup>TM</sup><sub>397</sub>. The potential  $\text{pH}_t$   
374 uncertainty based on the thermistor was calculated by using the absolute difference between the  
375 thermistor derived temperature and that measured by the SBE 16plusV2 ( $T_{\text{diff}}$ ) from the OARC  
376 test tank deployments and the Kasitsna Bay SeaFETs<sup>TM</sup><sub>395, 396</sub> against the Seldovia data sonde 10  
377 km away. Finally, an average inter-sensor variability uncertainty term was calculated as the  
378 difference between the two SeaFETs<sup>TM</sup><sub>395, 396</sub> deployed side-by-side in Kasitsna Bay after a  
379 single-point *in situ* calibration was performed. All uncertainty terms were calculated and collated  
380 based on our evaluations from the Alaska deployed SeaFETs<sup>TM</sup><sub>395, 396, 397</sub>, while SeaFET<sup>TM</sup><sub>268</sub>  
381 deployed at Sentry Shoal was only included when determining the accuracy uncertainty term.  
382 Due to the disparity between reference samples for the Kasitsna Bay SeaFETs<sup>TM</sup><sub>395, 396</sub> and  
383 Sentry Shoal SeaFET<sup>TM</sup><sub>268</sub> (two discrete reference samples) to that at the ASPH SeaFET<sup>TM</sup><sub>397</sub>  
384 (256 reference samples), only the average calculated difference (SeaFET<sup>TM</sup>  $\text{pH}_t$  – “true  $\text{pH}_t$ ”) for  
385 each calibration method and electrode was used from the APSH SeaFET<sup>TM</sup><sub>397</sub> and then collated  
386 with the other reference points from the Kasitsna Bay and Sentry Shoal SeaFETs<sup>TM</sup><sub>395, 396, 268</sub>.

## 387 2.5.2 $\text{pH}_t$ time series analysis

388

389 Final time series analysis was examined in the time and frequency domain using the Mathworks  
390 software MATLAB (V. 2016a). Power spectral density was determined via Welch’s method  
391 using the pwelch function in MATLAB. Time series data was resampled and linearly  
392 interpolated in order to compensate for the missing data points that occurred when sensors  
393 arbitrarily stopped sampling.

394

## 395 3 Results

396

### 397 3.1 Test tank and field conditions

398

399 Finalized (i.e., calibrated)  $\text{pH}_t$  values from the first test tank deployment produced two different  
400 values, of which each was dependent on whether the calibration coefficient from the header file  
401 or the disc file was selected, the result was a difference of ~0.0011 units for both the internal and  
402 external electrodes. Because sensors were stored in tris buffer that lacked the addition of bromide  
403 between tank deployments and before field deployments, an environmental conditioning period  
404 was required for each of the Alaska SeaFETs<sup>TM</sup><sub>395, 396, 397</sub> once submerged in their respective  
405 field sites. Thus, any determination of SeaFET<sup>TM</sup>  $\text{pH}_t$  accuracy and conditioning period from



406 tank deployments were inconclusive and will not be considered henceforth. No SeaFETs<sup>TM</sup><sub>395, 396,</sub>  
407 <sub>397, 268</sub> displayed signs of biofouling or low battery power upon recovery.

408

409 SeaFET<sup>TM</sup><sub>397</sub> deployed in parallel with the BoL at the APSH experienced a tank failure  
410 on 8 April 2017 resulting in the sensor's emergence for 24 h. In addition, missing temperature  
411 and salinity values resulted in gaps of pH<sub>t</sub> measurements over the entire deployment. The BoL  
412 experienced flow control issues when initial deployment occurred on 6 March 2017 and was not  
413 online until 18 April 2017 but, then, operated nearly consistently until 24 May 2017. All pH<sub>t</sub> and  
414 temperature comparisons were, therefore, made beginning on 18 April 2017.

415

416 Due to the *in situ* environmental conditioning period of the Kasitsna Bay SeaFETs<sup>TM</sup><sub>395,</sub>  
417 <sub>396,</sub> calibration was performed using the initial reference sample collected on 18 March 2017,  
418 03:00 UTC and again with the reference sample collected on 3 June 2017, 03:00 UTC. Due to  
419 high variance between duplicate reference samples (SD: 0.08 pH<sub>t</sub>) on 19 March 2017, 15:00  
420 UTC, this reference was discarded and not used for comparison or calibration. The Sentry Shoal  
421 SeaFET<sup>TM</sup><sub>268</sub> underwent one maintenance and cleaning procedure, including a battery change,  
422 during the ~5-month deployment (Table 1). One calibration sample (19 July 2016) and one  
423 reference sample (9 November 2016) were averaged from duplicate rather than triplicate  
424 replicates due to large variance from one of the replicate samples. The reference sample taken on  
425 23 August 2016, 17:00 UTC was discarded as temperature and salinity data were missing and  
426 SeaFET<sup>TM</sup><sub>268</sub> pH<sub>t</sub> could not be calculated. The final reference sample (UTC: 9 November 2016,  
427 17:05) was taken 5 min after SeaFET<sup>TM</sup><sub>268</sub> sampled on 9 November 2016, 17:00 UTC.

428

### 429 **3.2 Thermistor response: test tank deployment**

430

431 The internal thermistor amongst the SeaFETs<sup>TM</sup><sub>395, 396, 397</sub> had a difference of less than 0.2 °C  
432 over the entirety of the second and third tank deployments. All thermistor derived temperature  
433 values had good alignment with the SBE 16plusV2 temperature, and consistently recorded a  
434 slightly higher temperature. The discrepancy between the thermistor temperature and  
435 SBE16plusV2 was minimal, and reached a maximum of 0.378 (logged by SeaFET<sup>TM</sup><sub>395</sub>) during  
436 any time over all tank deployments. The average discrepancy, however, was ~0.21 °C when  
437 averaging across all SeaFETs<sup>TM</sup><sub>395, 396, 397</sub> and all times.

438

### 439 **3.3 Field performance**

440

441 SeaFET<sup>TM</sup><sub>397</sub> deployed alongside the BoL appeared stable throughout its entire deployment and  
442 tracked the pH<sub>t</sub> derived from the BoL well (Fig. 2). Errant spikes were present from both  
443 electrodes throughout periods before 18 April 2017, which were a result of plumbing changes  
444 that occurred to the APSH incoming seawater. On 10 April 2017 the internal thermistor, BoL  
445 temp, and BoL salinity fluctuated by 3 °C and 14, respectively, over a 12 h period. These  
446 anomalies were removed from analysis. Salinity remained relatively stable throughout the rest of  
447 the deployment and ranged from 30.0 – 32.1. The pH<sub>t</sub> uncertainty (SeaFET<sup>TM</sup> – “true” pH<sub>t</sub>)  
448 decreased, and the accuracy of the SeaFET's<sup>TM</sup><sub>397</sub> internal electrode improved once the *in situ*  
449 single-point and multi-point calibrations were performed with a RMSE decreasing from 0.5455  
450 pH<sub>t</sub> units under factory calibration, 0.0361 pH<sub>t</sub> units for *in situ* single-point calibration and  
451 0.0273 pH<sub>t</sub> units for the *in situ* multi-point calibration. The external electrode also improved



452 accuracy with *in situ* single-point and multi-point calibrations with an RMSE of 0.1077 under  
453 factory calibration, 0.0390 for *in situ* single-point calibration and 0.0388 for the *in situ* multi-  
454 point calibration (Fig. 2). There was a significant difference in the reduction of the  $\text{pH}_t$   
455 uncertainty for both the internal and external electrodes when utilizing *in situ* single-point and  
456 multi-point calibration coefficients compared to the factory calibration coefficients (Table 2). In  
457 addition, there was a significant decrease in the  $\text{pH}_t$  uncertainty when using the *in situ* multi-  
458 point calibration coefficients rather than the *in situ* single-point method for the internal electrode,  
459 but not for the external electrode (Table 2). The  $\text{pH}_t$  uncertainty of the internal electrode  
460 decreased from 0.0294 units with an *in situ* single-point calibration to 0.0224 units after an *in*  
461 *situ* multi-point calibration. It should be noted that the time alignment disparity which ranged  
462 from 0 – 120 s is not considered a significant source of discrepancy as only 4 sample points out  
463 of the 256 comparable points were  $> 0.03$  units (i.e., only 4 comparable points greater than the  
464 average  $\text{pH}_t$  uncertainty found after calibration) between any one 5 min sample taken by the  
465 BoL. The internal thermistor of SeaFET<sup>TM</sup><sub>397</sub> tracked the recorded BoL temperature trend fairly  
466 (Fig. 3), but had a greater magnitude discrepancy than its test tank deployment ( $\sim 0.21$  °C). On  
467 average, the thermistor temperature had an absolute difference of 2.83 °C (SD 0.35) from 18  
468 April 2017 – 6 June 2017, which would result in a  $\text{pH}_t$  uncertainty of  $\sim 0.044$  units. SeaFET<sup>TM</sup><sub>397</sub>  
469 was not fully submerged in the conical tank leaving the top portion susceptible to air temperature  
470 fluctuations which could have affected the thermistor readings.

471

472 The SeaFETs<sup>TM</sup><sub>395, 396</sub> in Kasitsna Bay improved their accuracy after an *in situ* single-  
473 point calibration was performed (Fig. 4), however, this was only the case when sensors were not  
474 conditioned as calibration performed after the conditioning period reduced accuracy (Fig. 5). It  
475 should be noted that only the  $\text{pH}_t$  recorded by both SeaFETs<sup>TM</sup><sub>395, 396</sub> at times of the reference  
476 samples had precise salinity and temperature (temperature and salinity recorded with reference  
477 sample rather than thermistor derived temperature) measurements as all other measurements  
478 were calculated from salinity measured by the data sonde 10 km away, and with temperature  
479 derived from the onboard thermistor. The  $\text{pH}_t$  recorded by the external electrode at a fixed  
480 salinity displayed little to no variance relative to  $\text{pH}_t$  calculated with data sonde salinity ( $< 0.02$   
481  $\text{pH}_t$  difference: average whether conditioned or non-conditioned to environment). The average  
482  $\text{pH}_t$  uncertainty from both SeaFETs<sup>TM</sup><sub>395, 396</sub> reduced by approximately half for the internal  
483 electrode when not conditioned to the environment after an *in situ* single-point calibration was  
484 performed (0.1072 and 0.1394 to 0.0475 and 0.0741 units, respectively), while the external  
485 electrode improved only minimally from 0.0988 and 0.0963 to 0.0610 and 0.0894 units,  
486 respectively (Fig. 4). When *in situ* single-point calibration was performed after the  
487 SeaFETs<sup>TM</sup><sub>395, 396</sub> were conditioned (i.e., calibrated with reference sample taken on 4 June 2017,  
488 03:00 UTC), the  $\text{pH}_t$  uncertainty for the internal electrode reduced only minimally from factory  
489 calibration: 0.1072 and 0.1394 to 0.0896 and 0.1240 units, respectively (Fig. 5a, b). Conversely,  
490 the  $\text{pH}_t$  error for the external electrode increased from 0.0988 and 0.0963 to 0.1011 and 0.1480,  
491 respectively (Fig 5c, d).

492

493 Both SeaFETs<sup>TM</sup><sub>395, 396</sub> displayed low inter-sensor variability for the internal electrode,  
494 and high for the external electrode after *in situ* single-point calibration was performed on sensors  
495 not conditioned to the environment (Fig. 6, gray circles). The mean anomaly between both  
496 SeaFETs<sup>TM</sup><sub>395, 396</sub> internal electrodes was 0.0525 units, whereas the external mean anomaly was  
497 0.145 units. When measurements taken before the sensor was conditioned to the environment



498 (blue shaded region Fig. 6) were removed from analysis, the mean anomaly changed by  $< 0.006$   
499 units for both electrodes. Inter-sensor variability for both electrodes once conditioned, and after  
500 *in situ* single-point calibration, was  $< 0.05$  units: 0.0409 and 0.0461 units for the internal and  
501 external electrodes, respectively (Fig. 6, black circles). When measurements recorded before the  
502 sensors were conditioned to the environment were removed (blue shaded region Fig. 10), the  
503 anomaly decreased further,  $< 0.015$  units for both electrodes.

504

505 Thermistor readings on both SeaFETs<sup>TM</sup><sub>395, 396</sub> tracked the temperature at the Seldovia  
506 site well, however errant spikes occurred around 18 April 2017 and again around 10 May 2017,  
507 and continued till the end of the deployment (Fig. 7). The absolute average difference between  
508 the thermistor values and the Seldovia data sonde was  $0.281$  °C (SD 0.295), nearly identical to  
509 the difference displayed during the test tank deployments, average  $0.21$  °C.

510

511 At Sentry Shoal, temperature and salinity seasonally fluctuated and ranged from  $8.71 -$   
512  $21.8$  °C and  $23.4 - 29.4$ , respectively. There was no clear distinction in greater accuracy between  
513 the internal and external electrodes after *in situ* single-point calibration was performed. While the  
514 external electrode did display a lower  $pH_t$  average uncertainty, this was based on only two  
515 reference points, one of which had a time discrepancy of 5 min (9 November 2016, 17:05 UTC).  
516 Only two reference samples were comparable against SeaFET<sup>TM</sup><sub>268</sub>  $pH_t$  due to the loss of salinity  
517 and temperature data on 23 August 2016, 17:00 UTC. Reference samples on 26 September 2016  
518 and 9 November 2016 were, therefore, compared using the new calibration coefficients  
519 determined after redeployment on 27 August 2016. The average  $pH_t$  uncertainty was  $< 0.0115$   
520 units for both electrodes (Fig. 8) compared to average  $pH_t$  uncertainties of 0.0244 and 0.0560  
521 units for the internal and external electrodes, respectively, if initial calibration coefficients from  
522 19 July 2016 were retained. The low  $pH_t$  uncertainty ( $< 0.0137$  units) determined after the *in situ*  
523 single-point calibration, however, was still greater than the average  $pH_t$  uncertainty under factory  
524 calibration:  $< 0.005$  units for both electrodes (Fig 8).

525

### 526 3.4 Spectral analysis

527

528 All SeaFETs<sup>TM</sup><sub>395, 396, 397, 268</sub> displayed a mixed semi-diurnal tidal response during all field  
529 deployments (Fig. 9). SeaFETs<sup>TM</sup><sub>395, 396</sub> at Kasitsna Bay had a stronger amplitude response at a  
530 frequency of two cycles  $d^{-1}$ , whereas SeaFET<sup>TM</sup><sub>397</sub> had a greater amplitude at one cycle  $d^{-1}$  (Fig.  
531 9a, c, d). All three SeaFETs<sup>TM</sup><sub>395, 396, 397</sub> in Alaskan waters had a strong amplitude signal of 1  
532 cycle every 21 days, with an addition signal of one cycle every three days for SeaFET<sup>TM</sup><sub>397</sub>. The  
533 amplitude signal for SeaFET<sup>TM</sup><sub>397</sub> shifted depending on source of measurement (BoL, internal or  
534 external electrode), however, all measurement sources followed the same frequency pattern (Fig  
535 9a). SeaFET<sup>TM</sup><sub>268</sub> displayed a strong signal at a frequency of zero as well as at one and two  
536 cycles  $d^{-1}$  (Fig 9a).

537

### 538 3.5 Intrinsic uncertainty and accuracy

539

540 Among the calculated potential sources of uncertainty in  $pH_t$ , inter-sensor variability (difference  
541 between SeaFET's<sup>TM</sup>  $pH_t$ ) and sensor accuracy produced the greatest uncertainty discrepancies  
542 for the internal and external electrodes under factory calibration (Fig. 10). The  $pH_t$  uncertainty  
543 (i.e., overall sensor accuracy) for the internal electrode reduced a greater degree than the external



544 electrode at every ordinal calibration method: factory, *in situ* single-point, to *in situ* multi-point  
545 calibration (Fig. 10). This was not the case for the external electrode, however, as the overall  $\text{pH}_t$   
546 accuracy was greater when factory calibration was used compared to an *in situ* single-point  
547 calibration was performed after the sensor was conditioned. The thermistor uncertainty (i.e.,  
548 uncertainty when calculating  $\text{pH}_t$  based on the thermistor temperature rather than a more accurate  
549 temperature gauge) produced a  $\text{pH}_t$  uncertainty of 0.0044 units, and was based on the recorded  
550 values by SeaFETs<sup>TM</sup><sub>395, 396</sub>. Even though the temperature-derived values from the thermistor of  
551 SeaFETs<sup>TM</sup><sub>395, 396</sub> were compared against a data sonde 10 km away, the average  $T_{\text{diff}}$  values were  
552 consistent with the  $T_{\text{diff}}$  calculated from the test tank deployments (within 0.07°C) and, therefore,  
553 provided an adequate resolution to determine a thermistor uncertainty value.

554

#### 555 4 Discussion

556

557 Obtaining accurate and precise measurements of pH in nearshore coastal waters is crucial for  
558 understanding changing trends, dynamics, and current baselines of acidification in these—  
559 “susceptible to change”—marine domains. For dynamic nearshore systems, the current standard  
560 of OA weather (carbonate chemistry variability on timescales of days to months) accuracy  
561 should have an uncertainty no greater than 0.02 pH units according to the Global Ocean  
562 Acidification Observing Network (Newton et al. 2015). Previous evaluations of the SeaFET<sup>TM</sup>  
563 sensor package have demonstrated accuracy for both electrodes to be better than 0.02 pH units,  
564 with a range between 0.01 – 0.04 units for the internal electrode in more dynamic environments  
565 (Bresnahan et al., 2014; Gonski, 2018; Martz et al., 2010). Based on our findings, we observed  
566 an accuracy range of 0.009 – 0.148  $\text{pH}_t$  units after sensors were conditioned and *in situ* single-  
567 point or multi-point calibrations were performed for the internal and external electrodes. This  
568 range decreased when SeaFETs<sup>TM</sup><sub>395, 396</sub> from Kasitsna Bay were calibrated with reference  
569 samples taken at initial deployment (i.e., non-conditioned to environment). For SeaFET<sup>TM</sup><sub>397</sub>, the  
570 internal electrode’s accuracy was nearly identical to that of the external electrode after an *in situ*  
571 multi-point calibration (Fig. 2), suggesting that the internal electrode can produce a highly  
572 precise  $\text{pH}_t$  measurement comparable to the BoL with an accuracy meeting the standards of the  
573 OA weather measurements (Newton et al. 2015). This is not to suggest that the SeaFET<sup>TM</sup> can  
574 replace the BoL, particularly because the BoL can capture multiple carbonate chemistry  
575 measurements thereby fully constraining the system and identifying potential decoupling of the  
576 carbonate system in estuarine waters (Bandstra et al., 2006; Hales et al., 2016). Nonetheless, the  
577 SeaFET<sup>TM</sup> can provide an accurate measurement of  $\text{pH}_t$  in nearshore waters when SeaFET<sup>TM</sup>  
578 operation is executed with high precision.

579

580 SeaFETs<sup>TM</sup><sub>397, 268</sub> deployed at the APSH and at Sentry Shoal displayed the lowest  
581 uncertainty and greatest precision of  $\text{pH}_t$  measurements (Fig. 2 and 8). In both instances, the  
582 SeaFETs<sup>TM</sup><sub>397, 268</sub> were adequately conditioned (i.e., subjected to *in situ* conditions for ~50 days)  
583 before calibration was performed. The greater overall accuracy displayed by the SeaFET<sup>TM</sup><sub>268</sub> at  
584 Sentry Shoal may be due to the fact that the sensor was exposed to *in situ* conditions for a longer  
585 period of time and re-calibrated multiple times to the same environment. Further, calibration and  
586 reference sample  $\text{pH}_t$  was derived from  $\text{TCO}_2$  and  $p\text{CO}_2$  processed by the BoL at Sentry Shoal  
587 and from  $p\text{CO}_2$  (also measured by BoL) and the TA-salinity relationship (Evans et al. 2015) at  
588 the APSH. It is unclear as to why the sensor accuracy of both Kasitsna Bay SeaFETs<sup>TM</sup><sub>395, 396</sub>  
589 was substantially less than the SeaFETs<sup>TM</sup><sub>397, 268</sub> at the APSH or Sentry Shoal. A potential reason



590 for the low accuracy may be that sensors were calibrated at a reference point that was extreme  
591 relative to the time series  $\text{pH}_t$  signal—that is, calibrated at a time of high variability. In this case,  
592 performing an *in situ* multiple-point calibration could have reduced the uncertainty and increased  
593 the accuracy. While previous studies have found that collection and preservation of calibration  
594 and reference samples can result in a decrease in accuracy depending on operator experience  
595 (McLaughlin et al., 2017), the operator in this study was considered to have substantial  
596 experience conducting such operations used in this evaluation. In addition, given the increased  
597  $\text{pH}_t$  variability over a short temporal period—which can be seen at the end of the Kasitsna Bay  
598 deployment (Fig. 4 and 5)—and the low discrepancy between duplicate reference samples, the  
599 former reasoning (i.e., calibrated to an extreme reference point) is a more reasonable explanation  
600 for the reduced accuracy by the Kasitsna Bay SeaFETs<sup>TM</sup><sub>395, 396</sub> than operator experience. We re-  
601 iterate here that reference sample temperature and salinity were used to calculate SeaFET<sup>TM</sup>  $\text{pH}_t$   
602 at the time points in which sensor  $\text{pH}_t$  and reference sample  $\text{pH}_t$  were compared, thus salinity  
603 was not a confounding factor.

604

605

606 Despite the lower accuracy of the Kasitsna Bay SeaFETs<sup>TM</sup><sub>395, 396</sub>, the two sensors  
607 provided a better insight of inter-sensor variability for non-conditioned to the environment and  
608 conditioned electrodes. After *in situ* single-point calibration for conditioned sensors, the average  
609 inter-sensor variability decreased for the internal electrode by ~80%, and >300% for the external  
610 electrode (Fig. 6). The inter-sensor variability reported here was still greater than previous  
611 findings (Kapsenberg et al., 2017), however, the comparison made in this study was done in the  
612 field compared to controlled laboratory conditions as in Kapsenberg et al. (2017). And while  
613 non-homogenized water could lead to anomalies in  $\text{pH}_t$  measurements by the Kasitsna Bay  
614 SeaFETs<sup>TM</sup><sub>395, 396</sub>, it is unlikely that water was consistently non-homogenized over the entirety of  
615 a deployment at a distance of < 20 cm (distance between electrodes on each SeaFET<sup>TM</sup>).  
616 Furthermore, due to the dynamic nature of Kachemak Bay, where the tidal exchanges are  
617 extreme, averaging 4.73 m, it is unlikely that micro-heterogeneity of seawater is the driving force  
618 behind the observed differences in  $\text{pH}_t$  measurements that were observed between SeaFETs<sup>TM</sup><sub>395,</sub>  
619 <sub>396</sub>. There was a tradeoff for a decrease in inter-sensor variability, as the *in situ* single-point  
620 calibration performed after sensors were conditioned resulted in a decrease in accuracy compared  
621 to an *in situ* single-point calibration performed for sensors not conditioned to the environment. It  
622 should be noted that we do not consider salinity to be a potential source of uncertainty for inter-  
623 sensor variability because the  $\text{pH}_t$  difference using data sonde salinity compared to a fixed  
624 salinity resulted in an anomaly of < 0.005 units.

624

625

626 The Sentry Shoal SeaFET<sup>TM</sup><sub>268</sub> had the lowest average  $\text{pH}_t$  uncertainty for both electrodes  
627 after *in situ* single-point calibration was performed, however, these were still greater than the  $\text{pH}_t$   
628 uncertainty determined using the factory calibration coefficients. This specific example  
629 highlights two possibilities: (1) the role of inter-sensor variability, as this may be a coincidental  
630 case given the uncertainty observed when quantifying inter-sensor variability, and (2) the  
631 influence of variance within a calibration sample set. For the case of SeaFET<sup>TM</sup><sub>268</sub>, the replicate  
632 calibration samples collected on 19 July 2016 and 2 September 2016 for the first and second  
633 deployments had standard deviations of 0.016 and 0.005  $\text{pH}_t$  units, respectively. For instances of  
634 generally close agreement between factory and *in situ* calibrated data, the variance in the  
635 calibration sample set may contribute to better agreement between factory calibrated sensor  $\text{pH}_t$   
data and average discrete sample  $\text{pH}_t$  measurements. It should also be noted that pre-deployment



636 calibration can provide highly accurate measurements by the Honeywell Durafet (internal  
637 electrode), however, matching exact conditions to those at the field site are necessary (Johnson et  
638 al., 2017), and this was not likely the case for the factory provided calibration coefficients.  
639

640 The evaluation of SeaFET<sup>TM</sup> performance presented here corroborates and contrasts with  
641 previous studies examining the overall accuracy and precision of pH<sub>t</sub> measurements made by  
642 these oceanographic instruments. While the accuracy of two SeaFETs<sup>TM</sup><sub>397, 268</sub> fall well within  
643 the range determined from previous studies, the accuracy of SeaFETs<sup>TM</sup><sub>395, 396</sub> at Kasitsna Bay  
644 lay outside the bounds of what has been report in the primary literature (Bresnahan et al., 2014;  
645 Gonski et al., 2018; Johnson et al., 2017; Kapsenberg et al., 2017; Martz et al., 2010).  
646 Nevertheless, it is relevant to report the potential uncertainties possible when operating  
647 SeaFETs<sup>TM</sup> as a multitude of factors can influence the overall accuracy (e.g., operator, sample  
648 preservation, electrode conditioning, calibration measurements), therefore, the potential  
649 uncertainties calculated in this study represent the upper limit of an average uncertainty compiled  
650 from four different SeaFETs<sup>TM</sup> (Fig. 10). The utility of such an analysis provides a confidence in  
651 SeaFET<sup>TM</sup> operation, and highlights all the potential uncertainties that need to be considered  
652 when deploying the sensors in the field. For example, we have included a thermistor uncertainty  
653 term determined from the test tank and field deployments of the Alaska SeaFETs<sup>TM</sup><sub>395, 396, 397</sub>,  
654 even though a suitable solution around this issue would be to apply an offset to the thermistor  
655 temperature given it was compared to more robust temperature measurements conducted before  
656 field deployment. It should be noted, that in this case, the thermistor uncertainty observed from  
657 SeaFET<sup>TM</sup><sub>397</sub> against the BoL was excluded as the lag time between thermistor response and tank  
658 residence time likely confounded the comparison. The potential pH<sub>t</sub> uncertainties presented here  
659 should serve as a guide for SeaFET<sup>TM</sup> operators in order to better understand the source of an  
660 uncertainty and take the necessary steps to improve SeaFET<sup>TM</sup> measurements. Bresnahan et al.  
661 (2014) acknowledged that relying on the SeaFET<sup>TM</sup> for an accurate pH measurement should be  
662 viewed cautiously if additional biogeochemical sensors are not co-deployed to cross-validate the  
663 stability and accuracy of the SeaFET's<sup>TM</sup> electrodes, therefore, being fully aware of all the  
664 potential uncertainties presented here will only further aid SeaFET<sup>TM</sup> operators.  
665

666 The time series data provided by the SeaFET<sup>TM</sup> deployments in this study have expanded  
667 the scope of spatial pH<sub>t</sub> variability along the North American west coast. The SeaFETs<sup>TM</sup><sub>395, 396</sub>  
668 deployed in Kasitsna Bay provide some of the first high temporal resolution measurements of  
669 pH<sub>t</sub> in this region. During this spring deployment, it appears that semi-diurnal tidal fluctuations  
670 are the dominant contributor to pH<sub>t</sub> variability with an additional cycle occurring every 21 days  
671 coinciding with the seasonal spring and neap tides (Fig. 9). The SeaFET<sup>TM</sup><sub>268</sub> at Sentry Shoal  
672 also displays a strong pH<sub>t</sub> response to the semi-diurnal mixed tidal cycle. A strong signal is also  
673 present at a frequency of zero, and is likely a result of the long, across-season, time series. That  
674 is, over the course of the entire deployment which went from summer into late fall, seasonal  
675 drivers of pH<sub>t</sub> (e.g., decrease in water temperature) confounded repetitive frequency patterns. In  
676 addition, Sentry Shoal may have a weaker tidal signature relative to other pH<sub>t</sub> modulators that do  
677 not follow a cyclical pattern such as water mass intrusion, inconsistent metabolic cycles from the  
678 end of summer into the fall season, and a shift to the rainy season.  
679

680 As an elaboration on the power spectral density analysis, we suggest this form of  
681 frequency analysis can be utilized to better understand the system in which a SeaFET<sup>TM</sup> is



682 deployed, thus informing the operator as to what the drivers of their system are, and when to  
683 calibrate the sensor. It is possible that in a highly dynamic setting, the sensor could re-condition  
684 over time periods not resolved in a multi-point calibration sampling scheme, and this could  
685 enhance sensor inaccuracies. For example, in Kasitsna Bay, a strong semi-diurnal tide cycle was  
686 present, so upon redeployment in this area, if possible, the best calibration approach would be an  
687 *in situ* multi-point calibration between the M2 cycle. Alternatively, if the system is not driven by  
688 a strong tidal signature (e.g., non-coastal region), an *in situ* single point calibration may be a  
689 reasonable approach.

690

## 691 **5 Conclusion**

692

693 The following evaluation of the Sea-Bird SeaFET™ helped elucidate the overall  
694 accuracy and highlighted the potential uncertainties and pitfalls of operating and obtaining pH<sub>t</sub>  
695 measurements by the internal and external electrode pair. We found that the internal electrode  
696 provided the more robust measurement in nearshore estuarine waters when an *in situ* multi-point  
697 calibration was performed (Fig. 10). The quantified potential pH<sub>t</sub> uncertainty is based  
698 specifically on our findings, whereas further results may minimize this uncertainty given  
699 additional evaluations. However, the results here provide an upper limit of the pH<sub>t</sub> uncertainty  
700 that may be observed when operating a Sea-Bird SeaFET™. Further, high temporal resolution  
701 pH<sub>t</sub> measurements in nearshore Canadian and Alaskan waters provide a better understanding of  
702 the drivers modulating pH on short timescales. Given the application, the Sea-Bird SeaFET™  
703 can provide a reliable and accurate pH<sub>t</sub> measurement which can be utilized to broaden the  
704 coverage of understanding pH variability in nearshore and open-ocean waters.

705

## 706 **Acknowledgments**

707 The authors would like to thank Jeff Hetrick and Jacqueline Ramsey at the Alutiiq Pride  
708 Shellfish Hatchery for providing their facilities and services for this evaluation. We would also  
709 like to thank Angela Doroff at the Kasitsna Bay laboratory for providing facilities for SeaFET™  
710 deployments. Funding for this project was provided in part by the University of Alaska  
711 Fairbanks College of Fisheries and Ocean Sciences. WE and KP thank the Pacific Salmon  
712 Foundation and Environment Canada for providing the platform for deploying SeaFET 268, the  
713 University of Alaska Fairbanks Ocean Acidification Research Center for the long-term use of  
714 SeaFET 268, and the Tula Foundation for supporting their efforts with this work.

715

716

## 717 **References**

718 Bandstra, L., Hales, B. and Takahashi, T.: High-frequency measurements of total CO<sub>2</sub>: Method  
719 development and first oceanographic observations, *Mar. Chem.*, 100(1–2), 24–38,  
720 doi:10.1016/j.marchem.2005.10.009, 2006.

721 Barton, A., Hales, B., Waldbusser, G. G., Langdon, C. and Feely, R. A.: The Pacific oyster,  
722 *Crassostrea gigas*, shows negative correlation to naturally elevated carbon dioxide levels:  
723 Implications for near-term ocean acidification effects, *Limnol. Oceanogr.*, 57(3), 698–710,  
724 doi:10.4319/lo.2012.57.3.0698, 2012.





- 725 Bresnahan, P. J., Martz, T. R., Takeshita, Y., Johnson, K. S. and LaShomb, M.: Best practices for  
726 autonomous measurement of seawater pH with the Honeywell Durafet, *Methods Oceanogr.*, 9,  
727 44–60, doi:10.1016/j.mio.2014.08.003, 2014.
- 728 Caldeira, K. and Wickett, M. E.: Anthropogenic carbon and ocean pH, *Nature*, 425(6956), 365–  
729 365, doi:10.1038/425365a, 2003.
- 730 Chan, F., Barth, J. A., Blanchette, C. A., Byrne, R. H., Chavez, F., Cheriton, O., Feely, R. A.,  
731 Friederich, G., Gaylord, B., Gouhier, T., Hacker, S., Hill, T., Hofmann, G., McManus, M. A.,  
732 Menge, B. A., Nielsen, K. J., Russell, A., Sanford, E., Sevdjian, J. and Washburn, L.: Persistent  
733 spatial structuring of coastal ocean acidification in the California Current System, *Sci. Rep.*, 7(1),  
734 2526, doi:10.1038/s41598-017-02777-y, 2017.
- 735 Dickson, A. G., Sabine, C. L. and Christian, J. R.: Guide to Best Practices for Ocean CO<sub>2</sub>  
736 Measurements., Report, North Pacific Marine Science Organization. [online] Available from:  
737 <http://www.oceandatapactices.net:80/handle/11329/249>, 2007.
- 738 Duarte, C. M., Hendriks, I. E., Moore, T. S., Olsen, Y. S., Steckbauer, A., Ramajo, L.,  
739 Carstensen, J., Trotter, J. A. and McCulloch, M.: Is Ocean Acidification an Open-Ocean  
740 Syndrome? Understanding Anthropogenic Impacts on Seawater pH, *Estuaries Coasts*, 36(2),  
741 221–236, doi:10.1007/s12237-013-9594-3, 2013.
- 742 Ekstrom, J. A., Suatoni, L., Cooley, S. R., Pendleton, L. H., Waldbusser, G. G., Cinner, J. E.,  
743 Ritter, J., Langdon, C., van Hooijdonk, R., Gledhill, D., Wellman, K., Beck, M. W., Brander, L.  
744 M., Rittschof, D., Doherty, C., Edwards, P. E. T. and Portela, R.: Vulnerability and adaptation of  
745 US shellfisheries to ocean acidification, *Nat. Clim. Change*, 5(3), 207–214,  
746 doi:10.1038/NCLIMATE2508, 2015.
- 747 Evans, W., Mathis, J. T. and Cross, J. N.: Calcium carbonate corrosivity in an Alaskan inland  
748 sea, *Biogeosciences*, 11(2), 365–379, doi:10.5194/bg-11-365-2014, 2014.
- 749 Evans, W., Mathis, J. T., Ramsay, J. and Hetrick, J.: On the Frontline: Tracking Ocean  
750 Acidification in an Alaskan Shellfish Hatchery, *PLOS ONE*, 10(7), e0130384,  
751 doi:10.1371/journal.pone.0130384, 2015.
- 752 Feely, R. A., Alin, S. R., Newton, J., Sabine, C. L., Warner, M., Devol, A., Krembs, C. and  
753 Maloy, C.: The combined effects of ocean acidification, mixing, and respiration on pH and  
754 carbonate saturation in an urbanized estuary, *Estuar. Coast. Shelf Sci.*, 88(4), 442–449,  
755 doi:10.1016/j.ecss.2010.05.004, 2010.
- 756 Feely, R. A., Alin, S. R., Carter, B., Bednaršek, N., Hales, B., Chan, F., Hill, T. M., Gaylord, B.,  
757 Sanford, E., Byrne, R. H., Sabine, C. L., Greeley, D. and Juraneck, L.: Chemical and biological  
758 impacts of ocean acidification along the west coast of North America, *Estuar. Coast. Shelf Sci.*,  
759 183, Part A, 260–270, doi:10.1016/j.ecss.2016.08.043, 2016.
- 760 Gonski, S. F., Cai, W.-J., Ullman, W. J., Joesoef, A., Main, C. R., Pettay, D. T. and Martz, T. R.:  
761 Assessment of the suitability of Durafet-based sensors for pH measurement in dynamic estuarine



- 762 environments, *Estuar. Coast. Shelf Sci.*, 200(Supplement C), 152–168,  
763 doi:10.1016/j.ecss.2017.10.020, 2018.
- 764 Hales, B., Suhrbier, A., Waldbusser, G. G., Feely, R. A. and Newton, J. A.: The Carbonate  
765 Chemistry of the “Fattening Line,” Willapa Bay, 2011–2014, *Estuaries Coasts*, 1–14,  
766 doi:10.1007/s12237-016-0136-7, 2016.
- 767 Harris, K. E., DeGrandpre, M. D. and Hales, B.: Aragonite saturation state dynamics in a coastal  
768 upwelling zone, *Geophys. Res. Lett.*, 40(11), 2720–2725, doi:10.1002/grl.50460, 2013.
- 769 Hofmann, G. E., Smith, J. E., Johnson, K. S., Send, U., Levin, L. A., Micheli, F., Paytan, A.,  
770 Price, N. N., Peterson, B., Takeshita, Y., Matson, P. G., Crook, E. D., Kroeker, K. J., Gambi, M.  
771 C., Rivest, E. B., Frieder, C. A., Yu, P. C. and Martz, T. R.: High-Frequency Dynamics of Ocean  
772 pH: A Multi-Ecosystem Comparison, *Plos One*, 6(12), e28983,  
773 doi:10.1371/journal.pone.0028983, 2011.
- 774 Johnson, K. S., Plant, J. N., Coletti, L. J., Jannasch, H. W., Sakamoto, C. M., Riser, S. C., Swift,  
775 D. D., Williams, N. L., Boss, E., Haentjens, N., Talley, L. D. and Sarmiento, J. L.:  
776 Biogeochemical sensor performance in the SOCCOM profiling float array, *J. Geophys. Res.-*  
777 *Oceans*, 122(8), 6416–6436, doi:10.1002/2017JC012838, 2017.
- 778 Kapsenberg, L., Bockmon, E. E., Bresnahan, P. J., Kroeker, K. J., Gattuso, J.-P. and Martz, T.  
779 R.: Advancing Ocean Acidification Biology Using Durafet® pH Electrodes, *Front. Mar. Sci.*, 4,  
780 doi:10.3389/fmars.2017.00321, 2017.
- 781 Kapsenberg, L. and Hofmann, G. E.: Ocean pH time-series and drivers of variability along the  
782 northern Channel Islands, California, USA, *Limnol. Oceanogr.*, 61(3), 953–968,  
783 doi:10.1002/lno.10264, 2016.
- 784 Kapsenberg, L., Kelley, A. L., Shaw, E. C., Martz, T. R. and Hofmann, G. E.: Near-shore  
785 Antarctic pH variability has implications for the design of ocean acidification experiments, *Sci.*  
786 *Rep.*, 5, srep09638, doi:10.1038/srep09638, 2015.
- 787 Khoo, K. H., Ramette, R. W., Culberson, C. H. and Bates, R. G.: Determination of hydrogen ion  
788 concentrations in seawater from 5 to 40.degree.C: standard potentials at salinities from 20 to  
789 45%, *Anal. Chem.*, 49(1), 29–34, doi:10.1021/ac50009a016, 1977.
- 790 Lueker, T. J., Dickson, A. G. and Keeling, C. D.: Ocean pCO<sub>2</sub> calculated from dissolved  
791 inorganic carbon, alkalinity, and equations for K-1 and K-2: validation based on laboratory  
792 measurements of CO<sub>2</sub> in gas and seawater at equilibrium, *Mar. Chem.*, 70(1–3), 105–119,  
793 doi:10.1016/S0304-4203(00)00022-0, 2000.
- 794 Martz, T., Send, U., Ohman, M. D., Takeshita, Y., Bresnahan, P., Kim, H.-J. and Nam, S.:  
795 Dynamic variability of biogeochemical ratios in the Southern California Current System,  
796 *Geophys. Res. Lett.*, 41(7), 2496–2501, doi:10.1002/2014GL059332, 2014.
- 797 Martz, T. R., Connery, J. G. and Johnson, K. S.: Testing the Honeywell Durafet® for seawater  
798 pH applications, *Limnol. Oceanogr. Methods*, 8(5), 172–184, doi:10.4319/lom.2010.8.172, 2010.



- 799 Martz, T. R., Daly, K. L., Byrne, R. H., Stillman, J. H. and Turk, D.: Technology for ocean  
800 acidification research: needs and availability, *Oceanography*, 28(2), 40–47, 2015.
- 801 Mathis, J. T., Cross, J. N. and Bates, N. R.: Coupling primary production and terrestrial runoff to  
802 ocean acidification and carbonate mineral suppression in the eastern Bering Sea, *J. Geophys.*  
803 *Res. Oceans*, 116(C2), C02030, doi:10.1029/2010JC006453, 2011a.
- 804 Mathis, J. T., Cross, J. N. and Bates, N. R.: The role of ocean acidification in systemic carbonate  
805 mineral suppression in the Bering Sea, *Geophys. Res. Lett.*, 38(19), L19602,  
806 doi:10.1029/2011GL048884, 2011b.
- 807 Mathis, J. T., Pickart, R. S., Byrne, R. H., McNeil, C. L., Moore, G. W. K., Juranek, L. W., Liu,  
808 X., Ma, J., Easley, R. A., Elliot, M. M., Cross, J. N., Reisdorph, S. C., Bahr, F., Morison, J.,  
809 Lichendorf, T. and Feely, R. A.: Storm-induced upwelling of high pCO<sub>2</sub> waters onto the  
810 continental shelf of the western Arctic Ocean and implications for carbonate mineral saturation  
811 states, *Geophys. Res. Lett.*, 39(7), L07606, doi:10.1029/2012GL051574, 2012.
- 812 Mathis, J. T., Cross, J. N., Monacci, N., Feely, R. A. and Stabeno, P.: Evidence of prolonged  
813 aragonite undersaturations in the bottom waters of the southern Bering Sea shelf from  
814 autonomous sensors, *Deep-Sea Res. Part II-Top. Stud. Oceanogr.*, 109, 125–133,  
815 doi:10.1016/j.dsr2.2013.07.019, 2014.
- 816 Mathis, J. T., Cross, J. N., Evans, W. and Doney, S. C.: Ocean Acidification in the Surface  
817 Waters of the Pacific-Arctic Boundary Regions, *Oceanography*, 28(2), 122–135,  
818 doi:10.5670/oceanog.2015.36, 2015a.
- 819 Mathis, J. T., Cooley, S. R., Lucey, N., Colt, S., Ekstrom, J., Hurst, T., Hauri, C., Evans, W.,  
820 Cross, J. N. and Feely, R. A.: Ocean acidification risk assessment for Alaska’s fishery sector,  
821 *Prog. Oceanogr.*, 136, 71–91, doi:10.1016/j.pocean.2014.07.001, 2015b.
- 822 Matson, P. G., Martz, T. R. and Hofmann, G. E.: High-frequency observations of pH under  
823 Antarctic sea ice in the southern Ross Sea, *Antarct. Sci.*, 23(6), 607–613,  
824 doi:10.1017/S0954102011000551, 2011.
- 825 McLaughlin, K., Dickson, A., Weisberg, S. B., Coale, K., Elrod, V., Hunter, C., Johnson, K. S.,  
826 Kram, S., Kudela, R., Martz, T., Negrey, K., Passow, U., Shaughnessy, F., Smith, J. E., Tadesse,  
827 D., Washburn, L. and Weis, K. R.: An evaluation of ISFET sensors for coastal pH monitoring  
828 applications, *Reg. Stud. Mar. Sci.*, 12, 11–18, doi:10.1016/j.rsma.2017.02.008, 2017.
- 829 Newton J.A., Feely R. A., Jewett E. B., Williamson P. & Mathis J.  
830 2015. Global Ocean Acidification Observing Network: Requirements and Governance Plan.  
831 Second Edition, GOA-ON, [http://www.goa-on.org/docs/GOA-ON\\_plan\\_print.pdf](http://www.goa-on.org/docs/GOA-ON_plan_print.pdf).  
832
- 833 Newton, J., Devol, A., Alford, M., Mickett, J., Sabine, C. and Sutton, A.: Nanoos Contributions  
834 to Understanding Ocean Acidification, *J. Shellfish Res.*, 31(1), 327–327, 2012.
- 835 Orr, J. C., Fabry, V. J., Aumont, O., Bopp, L., Doney, S. C., Feely, R. A., Gnanadesikan, A.,  
836 Gruber, N., Ishida, A., Joos, F., Key, R. M., Lindsay, K., Maier-Reimer, E., Matear, R., Monfray,



- 837 P., Mouchet, A., Najjar, R. G., Plattner, G. K., Rodgers, K. B., Sabine, C. L., Sarmiento, J. L.,  
838 Schlitzer, R., Slater, R. D., Totterdell, I. J., Weirig, M. F., Yamanaka, Y. and Yool, A.:  
839 Anthropogenic ocean acidification over the twenty-first century and its impact on calcifying  
840 organisms, *Nature*, 437(7059), 681–686, doi:10.1038/nature04095, 2005.
- 841 Orr, J. C., J.-M. Epitalon, A. G. Dickson, and J.-P. Gattuso: Routine uncertainty propagation for  
842 the marine carbon dioxide system, *Marine Chemistry, in prep.*  
843
- 844 Riebesell, U. and Gattuso, J.-P.: Lessons learned from ocean acidification research, *Nat. Clim.*  
845 *Change*, 5(1), 12–14, doi:10.1038/nclimate2456, 2015.
- 846 Rudd, M. A.: What a Decade (2006–15) Of Journal Abstracts Can Tell Us about Trends in  
847 Ocean and Coastal Sustainability Challenges and Solutions, *Front. Mar. Sci.*, 4,  
848 doi:10.3389/fmars.2017.00170, 2017.
- 849 Steinhart, J. S. and Hart, S. R.: Calibration curves for thermistors, *Deep Sea Res. Oceanogr.*  
850 *Abstr.*, 15(4), 497–503, doi:10.1016/0011-7471(68)90057-0, 1968.
- 851 Sunda, W. G. and Cai, W.-J.: Eutrophication Induced CO<sub>2</sub>-Acidification of Subsurface Coastal  
852 Waters: Interactive Effects of Temperature, Salinity, and Atmospheric P-CO<sub>2</sub>, *Environ. Sci.*  
853 *Technol.*, 46(19), 10651–10659, doi:10.1021/es300626f, 2012.
- 854 Takeshita, Y., Martz, T. R., Johnson, K. S. and Dickson, A. G.: Characterization of an Ion  
855 Sensitive Field Effect Transistor and Chloride Ion Selective Electrodes for pH Measurements in  
856 Seawater, *Anal. Chem.*, 86(22), 11189–11195, doi:10.1021/ac502631z, 2014.
- 857 Uppström, L. R.: The boron/chlorinity ratio of deep-sea water from the Pacific Ocean, *Deep Sea*  
858 *Res. Oceanogr. Abstr.*, 21, 161–162, doi:10.1016/0011-7471(74)90074-6, 1974.
- 859 Waldbusser, G. G. and Salisbury, J. E.: Ocean Acidification in the Coastal Zone from an  
860 Organism's Perspective: Multiple System Parameters, Frequency Domains, and Habitats,  
861 *Annu. Rev. Mar. Sci.*, 6(1), 221–247, doi:10.1146/annurev-marine-121211-172238, 2014.
- 862 Yu, P. C., Matson, P. G., Martz, T. R. and Hofmann, G. E.: The ocean acidification seascape and  
863 its relationship to the performance of calcifying marine invertebrates: Laboratory experiments on  
864 the development of urchin larvae framed by environmentally-relevant pCO<sub>2</sub>/pH, *J. Exp. Mar.*  
865 *Biol. Ecol.*, 400(1–2), 288–295, doi:10.1016/j.jembe.2011.02.016, 2011.
- 866  
867  
868  
869  
870  
871  
872  
873  
874  
875



876 **Table 1.** Deployment regime of all four SeaFETs™ including deployment location, date, and  
 877 calibration methods performed. \*Non-controlled source water pumped directly from  
 878 Resurrection Bay, AK, USA.  
 879

Location (Tank or Field)	Date	SeaFET™ ID	Average reads frame <sup>-1</sup>	Frames Burst <sup>-1</sup>	Sampling Freq. (min)	Calibration method
APSH — <i>Tank</i>	5 – 8 October 2016	395, 396, 397	1	10	5	Factory
OARC — <i>Tank</i>	26 October – 3 November 2016	395, 396, 397	3	—	Continuous	Factory
OARC — <i>Tank</i>	26 January – 1 February 2017	395, 396, 397	1	10	180	Factory
APSH <i>Field*</i>	5 March – 6 June 2017	397	10	30	180	Factory, SP and MP <i>in situ</i>
Kachemak Bay <i>Field</i>	18 March – 4 June 2017	395, 396	10	30	180	Factory, SP <i>in situ</i>
Sentry Shoal <i>Field</i>	6 July – 23 August, 27 August – 28 November 2016	268	10	30	30	Factory, SP <i>in situ</i>

880  
881  
882  
883  
884  
885  
886  
887  
888  
889  
890  
891  
892  
893  
894  
895  
896  
897  
898  
899  
900  
901  
902  
903  
904  
905  
906



907 **Table 2.** One-way Analysis of variance comparing the  $pH_t$  error (SeaFET<sup>TM</sup>  $pH_t$  – BoL  $pH_t$ )  
 908 across calibration methods for both the internal and external electrodes onboard SeaFETs<sup>TM</sup><sub>268</sub> at  
 909 Sentry Shoal (factory calibration and *in situ* single-point calibration) and SeaFET<sup>TM</sup><sub>397</sub> at the  
 910 Alutiiq Pride Shellfish Hatchery (factory calibration, *in situ* single-point calibration, and *in situ*  
 911 multi-point calibration). Bold type denotes statistical significance.

Site	Electrode	Source	SS	df	MS	F	p-value
APSH	Internal	Fac Cal. Vs. Single-point	27.5	1	27.5	4.96E+04	<b>&lt; 0.001</b>
		Error	0.225	406	0.001		
		Total	27.7	407			
APSH	External	Fac Cal. Vs. Single-point	0.681	1	0.681	536	<b>&lt; 0.001</b>
		Error	0.516	406	0.001		
		Total	1.19	407			
APSH	Internal	Factory Cal. vs. Multi-point	28.3	1	28.3	6.19E+04	<b>&lt; 0.001</b>
		Error	0.185	406	0.001		
		Total	28.5	407			
APSH	External	Factory Cal. vs. Multi-point	0.692	1	0.692	539	<b>&lt; 0.001</b>
		Error	0.521	406	0.001		
		Total	1.21	407			
APSH	Internal	Single-point vs. Multi-point	0.005	1	0.005	15.0	<b>&lt; 0.001</b>
		Error	0.143	406	0.000		
		Total	0.148	407			
APSH	External	Single-point vs. Multi-point	0.000	1	0.000	0.040	0.843
		Error	0.415	406	0.001		
		Total	0.415	407			

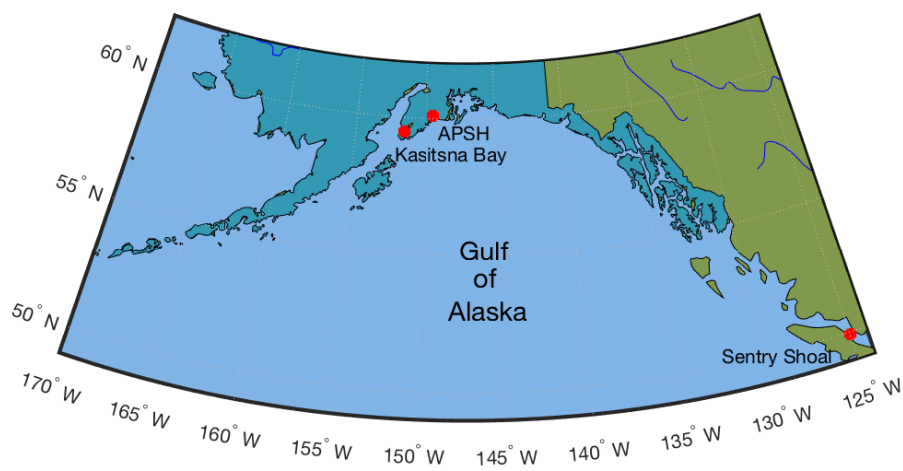
912  
 913  
 914  
 915  
 916  
 917  
 918  
 919  
 920  
 921  
 922  
 923  
 924  
 925  
 926  
 927  
 928  
 929  
 930  
 931  
 932  
 933  
 934  
 935  
 936



937 **Figure 1.**

938

939



940

941

942 Geographical map with locations of SeaFET™ field deployments along Alaska's, USA, south-  
943 central coast and one location in the Strait of Georgia, British Columbia, Canada.

944

945

946

947

948

949

950

951

952

953

954

955

956

957

958

959

960

961

962

963

964

965

966

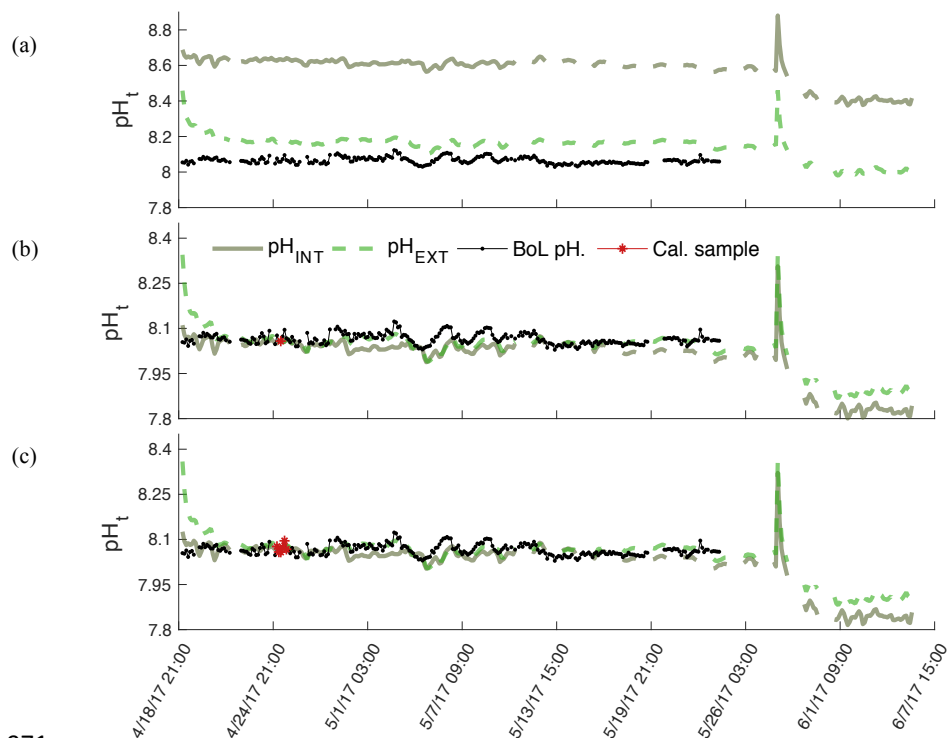
967

968



969 **Figure 2.**

970



971

972

973  $pH_t$  recorded by the internal (solid) and external (dashed) electrodes on SeaFET<sup>TM</sup><sub>397</sub> deployed in  
974 parallel with the BoL at the Alutiiq Pride Shellfish Hatchery.  $pH_t$  from both electrodes is shown  
975 when derived using factory calibration (FC) coefficients (panel a), *in situ* single-point (SC)  
976 calibration coefficients (panel b), and *in situ* multi-point (MC) calibration coefficients (panel c).  
977 Black solid line is  $pH_t$  derived from continuous  $pCO_2$  measurements recorded by the BoL and  
978 derived TA from the TA-S relationship (Evans et al. 2015). Red circles are the calibration points  
979 from the BoL data.

980

981

982

983

984

985

986

987

988

989

990

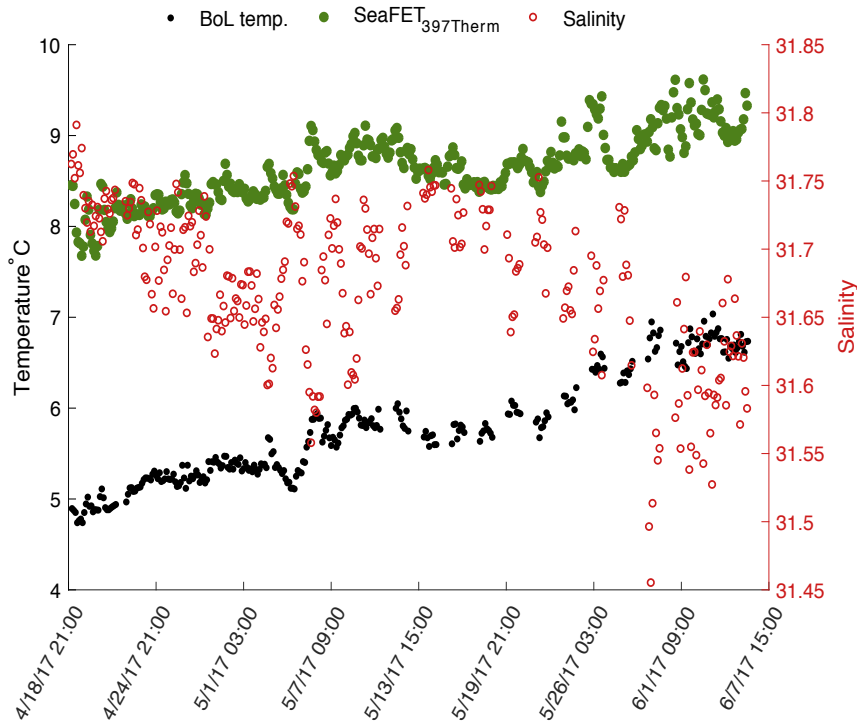
991

992





993 **Figure 3.**  
994

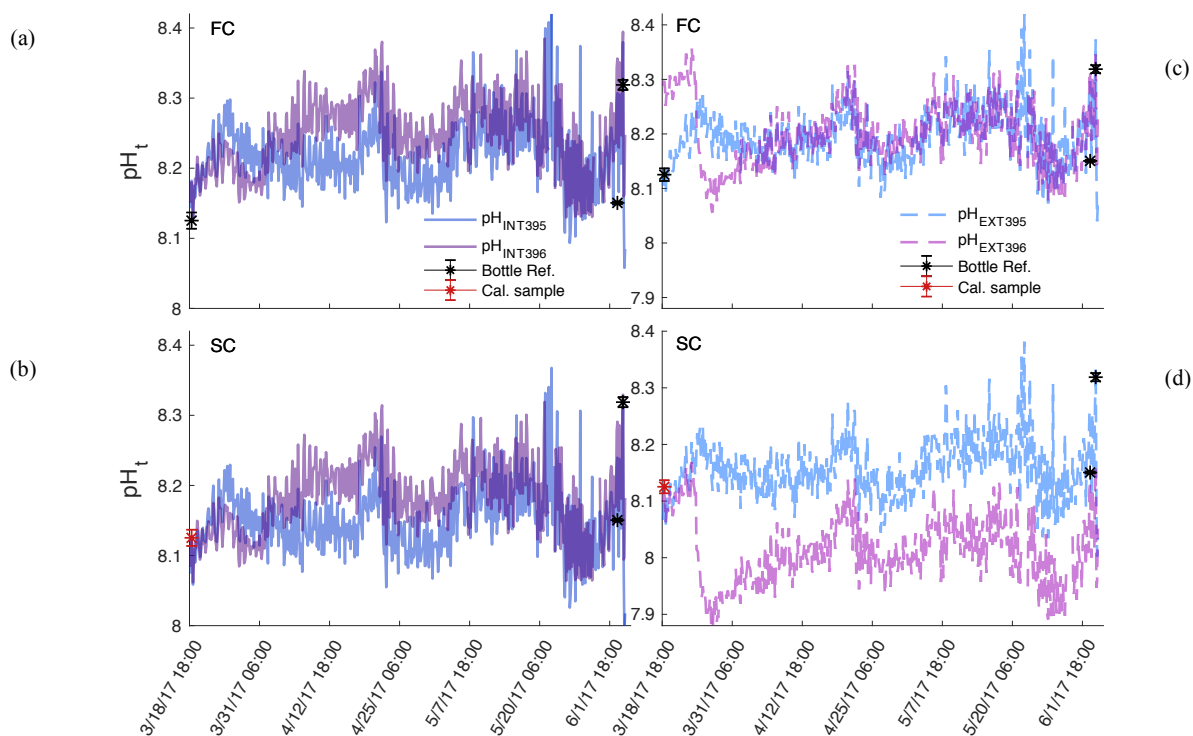


995  
996  
997  
998  
999  
1000  
1001  
1002  
1003  
1004  
1005  
1006  
1007  
1008  
1009  
1010  
1011  
1012  
1013  
1014  
1015  
1016

Temperature derived from the internal thermistor on SeaFET<sup>TM</sup><sub>397</sub> (green circles) and the temperature recorded by the BoL (black circles) at the Alutiiq Pride Shellfish Hatchery from late winter through spring 2017. Salinity (red circles) recorded by the BoL on the right y-axis.



1017 **Figure 4.**  
1018



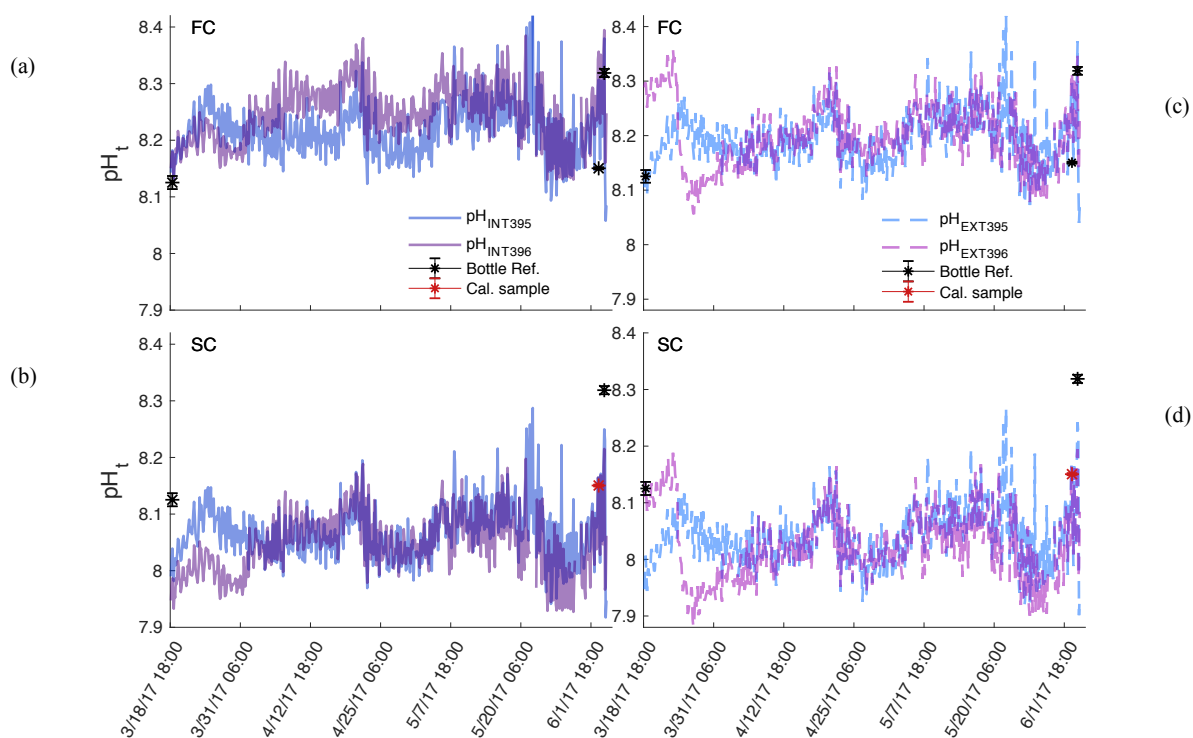
1019  
1020  
1021  
1022  
1023  
1024  
1025  
1026  
1027  
1028  
1029  
1030  
1031  
1032  
1033  
1034  
1035  
1036  
1037  
1038  
1039

Comparison of  $pH_t$  recorded by the internal (panel a and b) and external (panel c and d) electrodes on SeaFET<sup>TM</sup><sub>395</sub> (blue) and SeaFET<sup>TM</sup><sub>396</sub> (purple) before they were conditioned to the environment (non-conditioned) deployed in Kasitsna Bay, AK, based on calibration method: factory calibration (FC) and *in situ* single-point (SC) calibration. Discrete reference samples (black asterisks) and calibration sample (red asterisks) were collected 36 and 12 h pre-SeaFET<sup>TM</sup> recovery, and < 24 h post-deployment, respectively. Temperature and salinity measurements collected on reference and calibration samples were used to derive SeaFET<sup>TM</sup>  $pH_t$  at those given time points. All other SeaFET<sup>TM</sup>  $pH_t$  measurements use thermistor temperature and salinity logged by Kasitsna Bay data sonde.



1040  
1041  
1042

Figure 5.

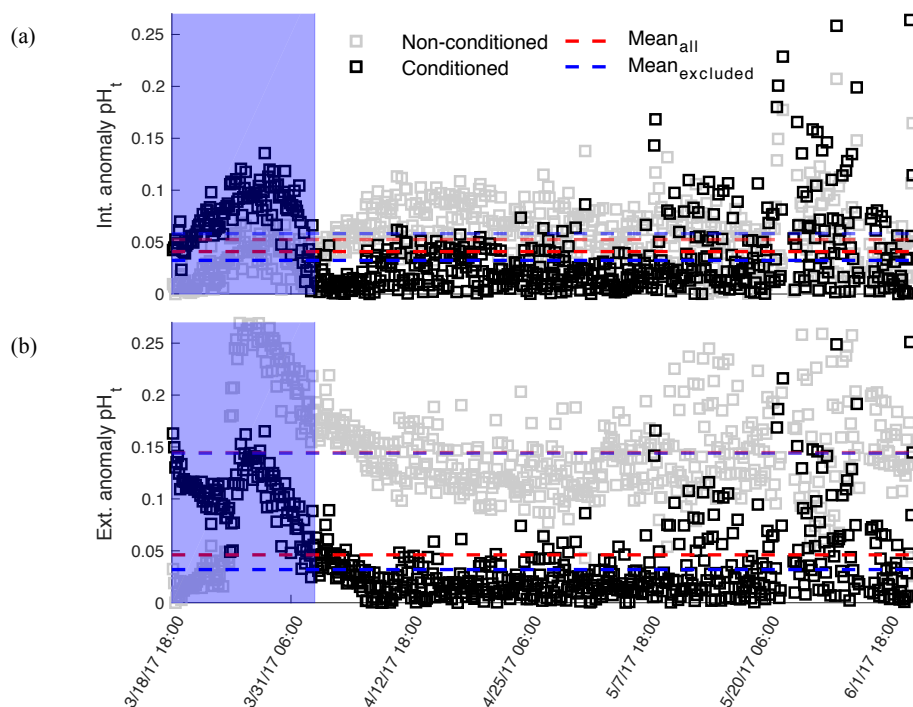


1043  
1044  
1045  
1046  
1047  
1048  
1049  
1050  
1051  
1052  
1053  
1054  
1055  
1056  
1057  
1058  
1059  
1060  
1061  
1062

Comparison of  $\text{pH}_t$  recorded by the internal (panel a and b) and external (panel c and d) electrodes on conditioned SeaFET<sup>TM</sup><sub>395</sub> (blue) and SeaFET<sup>TM</sup><sub>396</sub> (purple) deployed in Kasitsna Bay, AK, based on calibration method: factory calibration (FC) and *in situ* single-point (SC) calibration. Discrete reference samples (black asterisks) and calibration sample (red asterisks) were collected < 24 h post deployment and 12 h pre-SeaFET<sup>TM</sup> recovery, while calibration sample was collected 36 h pre-SeaFET<sup>TM</sup> recovery. Temperature and salinity measurements collected on reference and calibration samples were used to derive SeaFET<sup>TM</sup>  $\text{pH}_t$  at those given time points. All other SeaFET<sup>TM</sup>  $\text{pH}_t$  measurements use thermistor temperature and salinity logged by Kasitsna Bay data sonde.



1063  
 1064 **Figure 6.**  
 1065

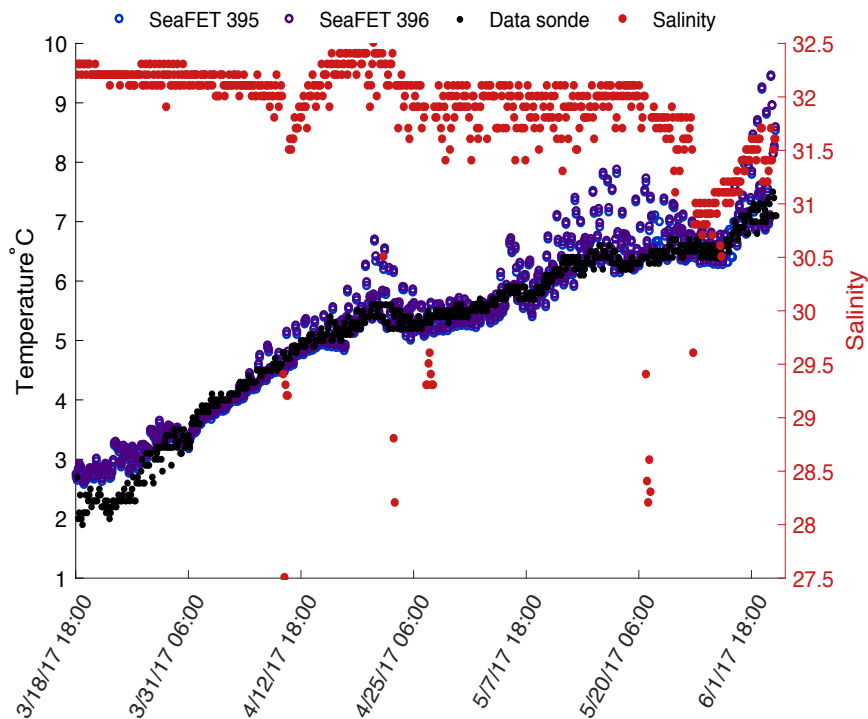


1066  
 1067  
 1068 Mean  $\text{pH}_t$  anomaly between *in situ* single-point calibrated SeaFET<sup>TM</sup><sub>395</sub> and SeaFET<sup>TM</sup><sub>396</sub>  
 1069 internal (panel a) and external (panel b) electrodes during parallel deployment in Kasitsna Bay,  
 1070 AK. Intra-anomaly comparison based on calibration sample taken at initial deployment (< 24 h  
 1071 non-conditioned, gray squares) and end of deployment (36 h pre-recovery, black squares).  
 1072 Shaded blue region indicates conditioning period. Data points in blue region omitted when mean  
 1073 anomaly was calculated (non-conditioned: transparent blue-dashed line; conditioned: bold blue-  
 1074 dashed line) compared to mean anomaly from entire data set (non-conditioned to environment:  
 1075 red-dashed line; conditioned: red- dashed line).  
 1076  
 1077  
 1078  
 1079  
 1080  
 1081  
 1082  
 1083  
 1084  
 1085  
 1086



1087  
1088  
1089

Figure 7.

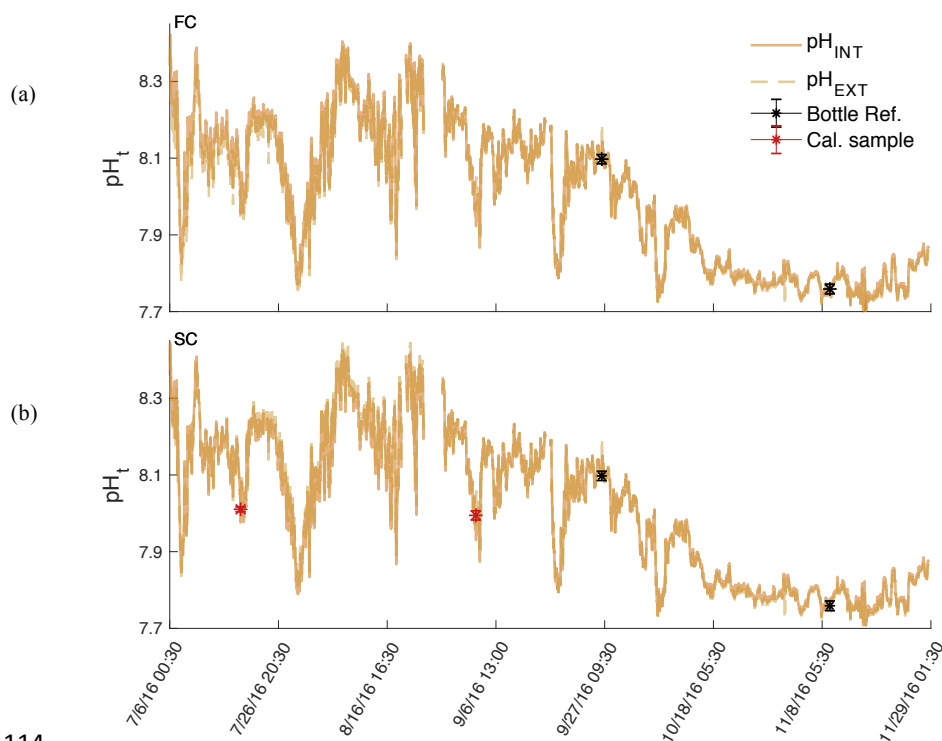


1090  
1091  
1092  
1093  
1094  
1095  
1096  
1097  
1098  
1099  
1100  
1101  
1102  
1103  
1104  
1105  
1106  
1107  
1108  
1109  
1110

Temperature derived from the internal thermistor on SeaFET<sup>TM</sup><sub>395</sub> (blue) and SeaFET<sup>TM</sup><sub>396</sub> (purple) compared against the temperature recorded by the Kachemak Bay National Estuarine Research Reserve data sonde. Salinity (Red circles) recorded by Kachemak Bay data sonde on the right y-axis.



1111  
1112 **Figure 8.**  
1113



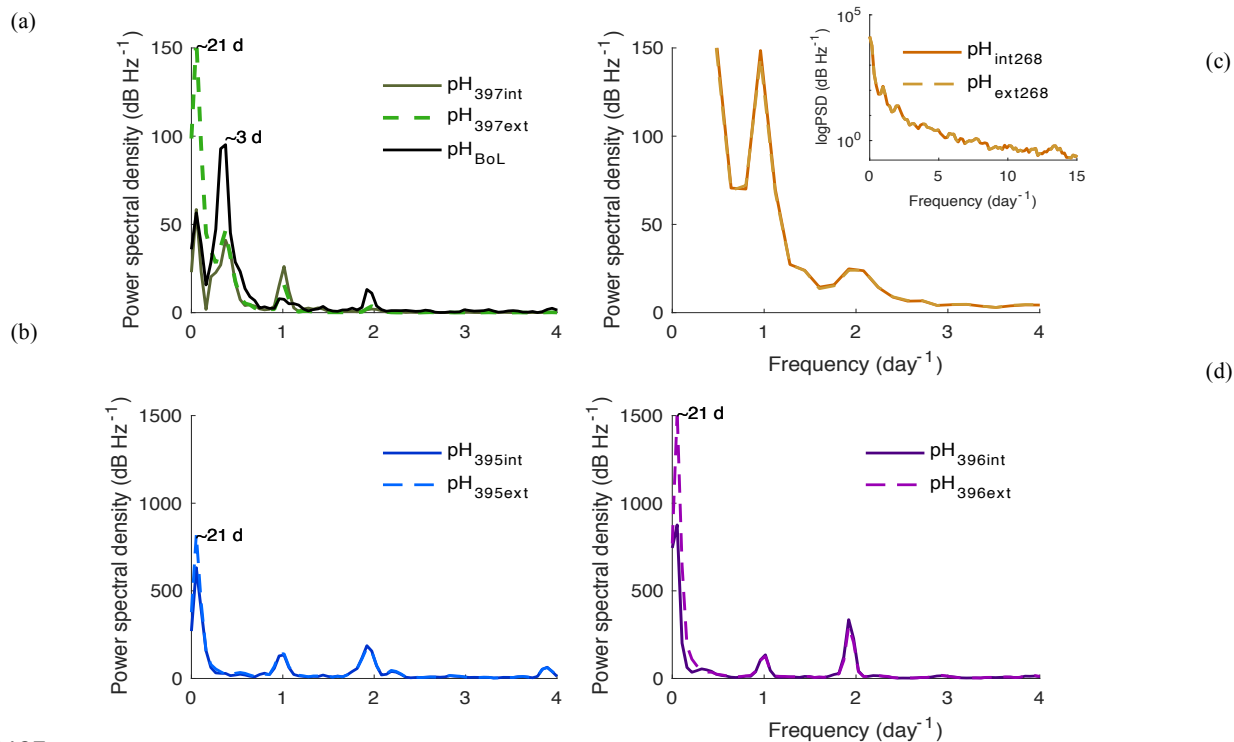
1114  
1115  
1116  $pH_t$  recorded by the internal (solid) and external (dashed) electrodes on SeaFET<sup>TM</sup><sub>268</sub> deployed at  
1117 the Sentry Shoal mooring.  $pH_t$  from both electrodes is shown when derived using factory  
1118 calibration (FC) coefficients (panel a) and *in situ* single-point (SC) calibration coefficients (panel  
1119 b). Black asterisks are references samples taken after initial calibration and recalibration (red  
1120 asterisk), where  $pH_t$  was derived from  $TCO_2$  and  $pCO_2$  measurements made on the BoL at the  
1121 Hakai Institute's Quadra Island Field Station.

1122  
1123  
1124  
1125  
1126  
1127  
1128  
1129  
1130  
1131  
1132  
1133  
1134



1135 **Figure 9.**

1136



1137

1138

1139 Power spectral density (PSD) analysis of  $\text{pH}_t$  in frequency per day for SeaFETs™ 397 (panel a),

1140 268 (panel b), 395 (panel c), and 396 (panel c). Inset in panel b is log base 10 transformed PSD

1141 analysis of same data set. All internal electrodes marked as solid colored lines while external

1142 electrodes are colored dashed lines. BoL data set marked as solid black line (panel a).

1143

1144

1145

1146

1147

1148

1149

1150

1151

1152

1153

1154

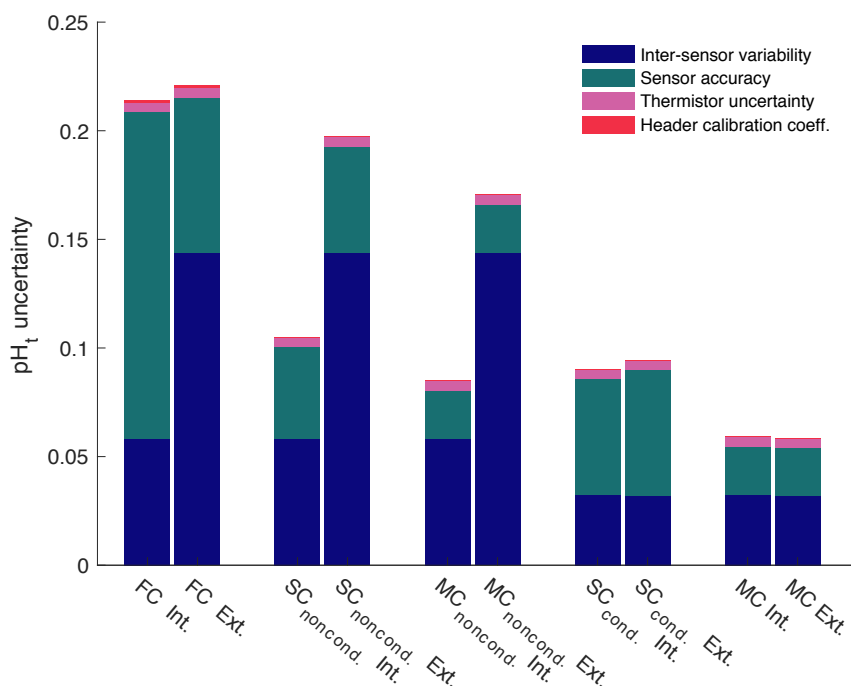
1155

1156

1157



1158 **Figure 10**  
 1159



1160  
 1161  
 1162  
 1163  
 1164  
 1165  
 1166  
 1167  
 1168  
 1169  
 1170  
 1171  
 1172  
 1173  
 1174  
 1175  
 1176

Quantified uncertainties based on field deployments of all Sea-Bird SeaFETs<sup>TM</sup> separated by electrode calibration method (FC: factory; SC: single-point; MC: multi-point), and calibration time for SeaFETs<sup>TM</sup> 395 and 396 (i.e., non-conditioned to environment and conditioned). pH<sub>t</sub> accuracy uncertainty calculated as the mean difference when comparing the absolute difference between reference samples and SeaFETs<sup>TM</sup> 395 (non-conditioned to environment and conditioned), 396 (non-conditioned to environment and conditioned), and 268 as well as the average absolute difference between SeaFET<sup>TM</sup> 397 and the BoL. Inter-sensor variability uncertainty determined by comparing SeaFETs<sup>TM</sup> 395 (non-conditioned to environment and conditioned) and 396 (non-conditioned to environment and conditioned), deployed side-by-side in Kasitsna Bay. Thermistor uncertainty is calculated pH<sub>t</sub> error when using thermistor derived temperature rather than external temperature sensor determined from SeaFETs<sup>TM</sup> 395 and 396. Header calibration coefficient uncertainty is the discrepancy in pH<sub>t</sub> when using SeaFETcom factory calibration coefficients from header file rather than disc file.